ABSTRACT

CALANTONI, JOSEPH. Discrete Particle Model for Bedload Sediment Transport in the Surf Zone. (Under the direction of Thomas G. Drake.)

Predicting the evolution of nearshore bathymetry from the highest uprush of the swash offshore to the location of wave breaking is a difficult problem of significant importance, with economic, legal, engineering, scientific, and military implications for coastal environments. Despite the apparent accessibility of the phenomena of interest, namely, the motion of sand under the forcing of waves and currents, the predictive capability of existing models for nearshore evolution is poor. A detailed study of the forces exerted on individual sand grains is undertaken in an effort to elucidate sediment transport mechanisms in the surf zone. New results indicate that fluid acceleration is a particularly important feature of surf zone transport; likewise, the processes of particle size segregation and the role of particle shape are newly explored. The study methodology employs computer simulations that describe the collective and individual motions of discrete particles immersed in a Newtonian fluid having essentially arbitrary density and viscosity. In this study all particle properties are those of quartz sand, and the fluid properties correspond to saltwater at 20° C. Such discrete-particle models, having a basis in molecular dynamics studies, have a broad range of applications in addition to the sedimentological one of interest here; for example, similar methodologies have been applied to traffic flow, schooling fish, crowd control, and other problems in which the particulate nature of the phenomenon is of critical importance.

DISCRETE PARTICLE MODEL FOR BEDLOAD SEDIMENT TRANSPORT IN THE SURF ZONE

by
JOSEPH CALANTONI

A dissertation submitted to the Graduate Faculty of
North Carolina State University
in partial fulfillment of the
requirements for the Degree of
Doctor of Philosophy

PHYSICS

Raleigh

2002

APPROVED BY:

_____ _____

_____ _____

Co-chair of Advisory Committee Co-chair of Advisory Committee

In Loving Memory of Daniel William Fry

BIOGRAPHY

I was born on July 22, 1972 in Allentown, PA. I attended Our Lady of Mount Carmel Elementary School and Pius X High School until 1986. I graduated from Nazareth Area High School in 1990. I finally received a B.S. in Physics from Penn State University in May 1996. Immediately, I entered graduate school in Physics at North Carolina State University. On November 11, 2002, I successfully defended this dissertation. I will begin tenure as a post-doc at the Naval Research Laboratory at NASA Stennis Space Center upon submission of this dissertation.

ACKNOWLEDGMENTS

I would like to thank my advisor, Thomas G. Drake, for his support and guidance over the years. I also would like to thank Peter K. Haff for valuable discussions that have helped shape the works in this dissertation.

I thank Richard R. Patty for supporting my decision to pursue research in geophysics and serving on my committee. I thank Lubos Mitas for serving as a committee co-chair.

I thank Christopher S. Thaxton for years of insightful discussions and for providing useful revisions of Chapters 4 and 5. I thank David M. Pierson for his tireless efforts to keep my computers running and secure.

Finally, I thank my family, especially my mother and father, for all their love and support over these years.

TABLE OF CONTENTS

LIST OF FIGURES

Chapter 1

Introduction

Predicting the evolution of nearshore bathymetry from the highest uprush of the swash offshore to the location of wave breaking is a difficult problem of significant importance, with economic, legal, engineering, scientific, and military implications for coastal environments. Despite the apparent accessibility of the phenomena of interest, namely, the motion of sand under the forcing of waves and currents, the predictive capability of existing models for nearshore evolution is poor. A detailed study of the forces exerted on individual sand grains is undertaken in an effort to elucidate sediment transport mechanisms in the surf zone. New results indicate that fluid acceleration is a particularly important feature of surf zone transport; likewise, the processes of particle size segregation and the role of particle shape are newly explored. The study methodology employs computer simulations that describe the collective and individual motions of discrete particles immersed in a Newtonian fluid having essentially arbitrary density and viscosity. In this study all particle properties are those of quartz sand, and the fluid properties correspond to saltwater at 20° C. Such discrete-particle models, having a basis in molecular dynamics studies, have a broad range of applications in addition to the sedimentological one of interest here; for example, similar methodologies have been applied to traffic flow, schooling fish, crowd control, and other problems in which the particulate nature of the phenomenon is of critical importance.

Transport of sand and coarser sediments by waves and currents in the nearshore environment is characterized by two dominant modes: bedload transport, in which grains collide, slide, bounce, and roll in close proximity to the bed, and suspended load, in which grains are lifted from the bed by fluid turbulence and suspended within the water column. This work focuses exclusively on a particular bedload transport phenomenon called sheet flow, which occurs under a limited but not atypical set of conditions observed in the surf zone during storms. Following a short introductory discussion of extant theories for bedload transport and sheet flow in particular, the remainder of the dissertation comprises a series of chapters either already published or soon-to-be submitted for publication. The chapters are presented in roughly chronological order.

Chapter 2 uses a discrete-particle modeling approach to address the concept of a local equilibrium beach slope [*Calantoni and Drake*, 1999]. The simulation predicts an equilibrium beach slope under conditions where the often-used transport model of *Bailard and Inman* [1981] is unable to make a prediction, revealing a shortcoming of their approach that is addressed in the following chapters.

Chapter 3 provides a detailed description of the discrete particle model, details the shortcomings of the energetics approach to bedload transport, and proposes an additional term in the *Bailard* [1981] bedload formula that accounts for effects of fluid acceleration in the transport process. A physical explanation for the additional term is presented and simulations are used to determine constants in the new theory.

Chapter 4 focuses on the effect of an arbitrarily sloping seabed on simulated bedload transport rates. One notable result is the occurrence of significant transport in the alongshore direction when the bed has a component of alongshore slope, independent of the fluid motion

provided that the critical threshold for motion is surpassed. The goal is to provide a vectorial bedload transport relation for surf zone transport that accounts for the effects of gravity on an arbitrarily oriented bed to the direction of the fluid forcing.

Chapter 5 introduces a significant enhancement of the discrete particle model that allows simulations to incorporate non-spherical particles, which are constructed from pairs of overlapping spheres which are hereafter referred to as composite particles. A suite of simulations demonstrates that varying the shape of composite particles in a systematic way allows quantitative prediction of the range of angles of repose observed in physical experiments for a variety of particle shapes and frictional properties.

1.1. Bedload Transport

Early work on bedload transport focused on steady flows characteristic of fluvial environments [*Meyer-Peter and Müller*, 1948; *Einstein*, 1950; *Bagnold*, 1966]. *Bailard* [1981] and *Bowen* [1980] independently constructed so-called energetics models for sediment transport in the surf zone based in part on *Bagnold's* theory [1966] for steady flows in rivers. For surf zone flows dominated by pervasive offshore flow, the Bagnold-Bowen-Bailard models (hereafter BBB) have demonstrated predictive skill [*Thornton et al.*, 1996; *Gallagher et al.*, 1998]. Unfortunately, several of the parameters in the BBB theories are difficult to evaluate, even with direct observations of bedload motion. In the surf zone, acoustic observations of bedload are now possible [e.g., *Traykovski et al.*, 1999; *Irish et al.*, 2002], but are very limited. At present, surf zone sediment transport is invariably inferred from changes in bathymetry via application of the sediment continuity equation and the compromising assumption that transport is alongshore uniform. A major goal of this work is

to provide a physically based model for bedload transport with no or few free parameters that can be tested with available field observations.

An alternative approach to modeling bedload transport based on kinetic theories for collisional grain flow has been proposed by *Jenkins and Hanes* [1998]. Their continuum approach to modeling granular flow treats the particle concentration in bedload as a continuous field [*Jenkins and Savage*, 1983; *Haff*, 1983]. *Hsu* [2002] generated a two-phase flow approach for bedload transport based on a kinetic theory approach and turbulent mixture theory. An informal, preliminary comparison of results from Hsu's model and the model used here at a recent meeting showed a number of qualitatively similar predictions, which may form the basis for collaborative work in the near future.

1.1.1. Sheet Flow Transport in the Surf Zone

Energetic waves in the surf zone often produce a transport regime called *sheet flow*, in which granular fluid is confined to a thin, nominally planar near bed layer on the order of a few mm to tens of mm thick with a well-defined upper surface. At sufficiently high shear rates and particle concentrations, *Bagnold's* [1956] pioneering experiments suggest that collisions between grains dominate momentum transport in the layer. Sheet flow transport is thought to be the dominant sediment transport process in the surf zone under energetic conditions, and thus the primary agent of nearshore bathymetric evolution during storms. Formulation of reliable predictive models for coastal morphologic evolution necessitates improvements in sediment transport formulae. The work presented here is focused on both improving parameterizations in existing models for bedload transport in the surf zone and further elucidating important transport mechanisms. The discrete-particle approach adopted here emphasizes the smallest scales of the problem, namely, the particle scale; the remainder

of the dissertation reveals the approach to have much promise for detailed understanding of sediment transport processes, which in turn form the basis for effective predictive models for beach evolution.

Chapter 2

Discrete-Particle Model for Bedload Transport: Implications for the Concept of Local Equilibrium Bed Slope in Oscillatory Flows

This chapter was co-authored by Thomas G. Drake and published in a similar form in the Proceedings of the International Association of Hydraulic Research on River, Coastal and Estuarine Morphodynamics, held September 6-10, 1999, in Genoa, Italy.

2.1. Introduction

A variety of sloping planar sediment surfaces typically occur in the surf zone, from the offshore-sloping swash zone to bed form surfaces sloping in all directions to bars having both onshore- and offshore-directed slopes. It is exceedingly difficult to make field measurements of bedload transport in the surf zone, let alone to determine the effect of a sloping bed on transport. Even controlled laboratory measurements of bedload transport over a sloping bed are uncommon [see *Damgaard et al.*, 1997]. On the other hand, discrete-particle computer simulations of bedload sediment transport predict bedload transport rates, segregation of grains by size and density, dispersion of grains and a variety of other transport phenomena difficult to study in the nearshore environment. This paper uses such simulations to predict bedload transport over a non-horizontal planar bed under oscillatory flow

conditions, and to address the implications of simulation predictions for the concept of a local equilibrium bed slope. The local equilibrium bed slope is that slope for which there is a local balance in transport, such that the onshore flux of sediment equals the offshore flux [e.g., *Inman and Bagnold*, 1963]. This paper does not address the generation of an equilibrium beach profile, which has been the subject of extensive study [e.g., *Dean*, 1977; *Inman et al.*, 1993, among many others].

Our simulations raise questions about the validity of the local equilibrium bed slope concept in many natural situations of interest; in particular, our simulations predict a slope of several degrees for certain commonly observed nearshore waveforms, whereas existing energetics-based models [*e.g.*, *Bagnold*, 1963, 1966; *Bowen*, 1980; *Bailard and Inman*, 1981] predict a local equilibrium bed slope of zero.

2.2. Simulation Models

Discrete-particle computer simulation models based on molecular-dynamics-like models for flowing granular materials [*Drake and Walton*, 1995] are used to simulate bedload transport of grains having nearly arbitrary diameter, density, elastic and frictional properties. Bedload transport rates predicted with the present model [*Calantoni and Drake*, 1998*a;b*] compare favorably with available experimental data for bedload transport of coarse sand in an oscillatory flow tunnel [*King*, 1991].

2.2.1. Particle Model

Velocities and positions of discrete spherical particles are obtained by integrating Newton's equations of motion at small time steps, and an analogous set of equations for the torques on the spheres is solved to provide their spins and orientations. Forces on particles

consist of particle-particle forces; particle-fluid forces; and pressure-gradient and gravitational body forces. Normal and tangential forces generated between contacting spheres are based on approximations [*Walton and Braun*, 1986*a;b*] to theoretical models for identical, homogeneous Hertzian elastic spheres developed by *Mindlin and Deresiewicz* [1953]. Fluid-particle interactions consist of buoyancy, drag and added mass forces. The coefficients of drag and added mass depend on the volume concentration of particles in the fluid.

2.2.2. Discrete-fluid model

A discrete-fluid model drives transport in the simulation (Figure 2.1). Pressure-gradient forces generated by the idealized progression of a surface gravity wave accelerate a stack of thin horizontal layers of fluid and the spherical particles embedded within them. Linear wave theory is used to determine the fluid pressure gradients at the bed [*Guza and Thornton*, 1980]. Because dimensions of the simulation volume are small, fluid pressure gradients within the volume are approximately constant, and thus closely resemble those in a laboratory flow tunnel. Fluid layers exchange momentum via an eddy viscosity determined from a mixing-length model. Each layer exerts buoyancy, drag and added-mass forces on particles embedded within it; particles exert equal and opposite forces on the fluid layers, thus fully coupling fluid and sediment motion. Although turbulence is implicit in a mixing-length approach, the fluid velocity within each layer is constant. The layer model inherently suppresses development of such bed features as ripples; however, under sheet flow conditions local bed topography is nominally planar.

Periodic boundaries are used in both the cross-shore and alongshore directions; particles exiting any side of the calculational volume are reintroduced with identical velocity

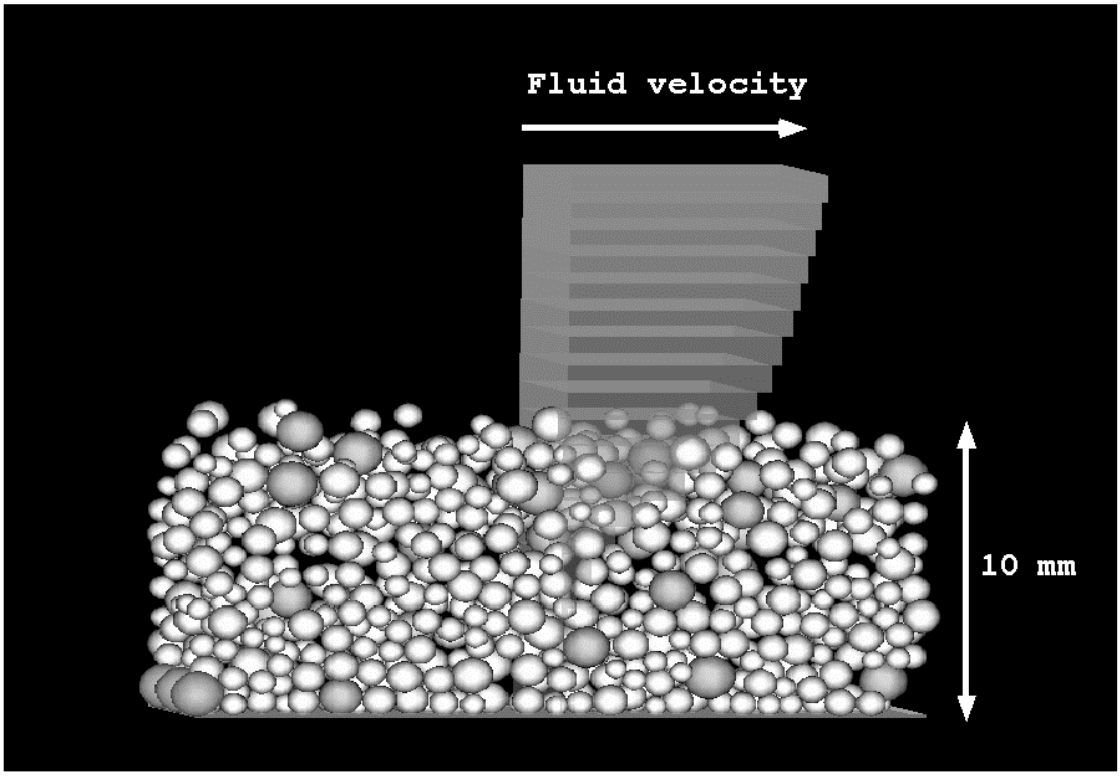

Figure 2.1. Snapshot from a typical simulation. The fluid is modeled as discrete slabs constrained to move parallel to the bed. Length of the slabs is proportional to fluid velocity. Dark grains are those larger than about 1.5 mm diameter to aid visualization of particle sorting processes. Periodic boundaries are used in both the on-offshore and alongshore directions; large grains are fixed to a smooth basal plane to prevent bulk sliding of the granular assemblage.

and rotation at the opposite side of the volume. The lower boundary of the calculational volume is a smooth plane with several fixed spheres to prevent wholesale sliding of the granular assemblage. The initial particle configuration is generated by gravitational settling of particles from a regular lattice into the calculational volume. Although larger particles settle more rapidly than smaller ones, the relatively high concentration effectively hinders size sorting during the settling process.

2.2.3. Comparisons with King's Experiments

King's [1991] oscillatory flow tunnel experiments using 1.1 mm mean diameter quartz sand in fresh water provide mean total sediment transport rates for half-cycle oscillatory flows under sinuosoidal and other waveforms in both horizontal and tilted-bed configurations. The model consistently reproduces results obtained by King to within about 20% [*Calantoni and Drake*, 1998a,b]. Our simulation approach is untested, at present, for finer-grained particles used in a number of other experiments.

2.2.4. Waveforms

The three different waveforms simulated are generated using a truncated Fourier series expansion for a sawtooth wave

$$u(t,f) = u_o \sum_{k=1}^{5} 2^{1-k} \cos\left(kwt + (k-1)f\right) \qquad (2.1)$$

In equation (2.1) the period $T = 2p/w = 6$ s is fixed for all waveforms. The waveform parameter f is set to 0, $p/4$ and $p/2$ to generate three wave shapes typical of nearshore waves. Adjusting u_o creates a time series having a desired maximum velocity; all of the waveforms simulated here have a maximum velocity of 1 m s^{-1}. Time series of velocity,

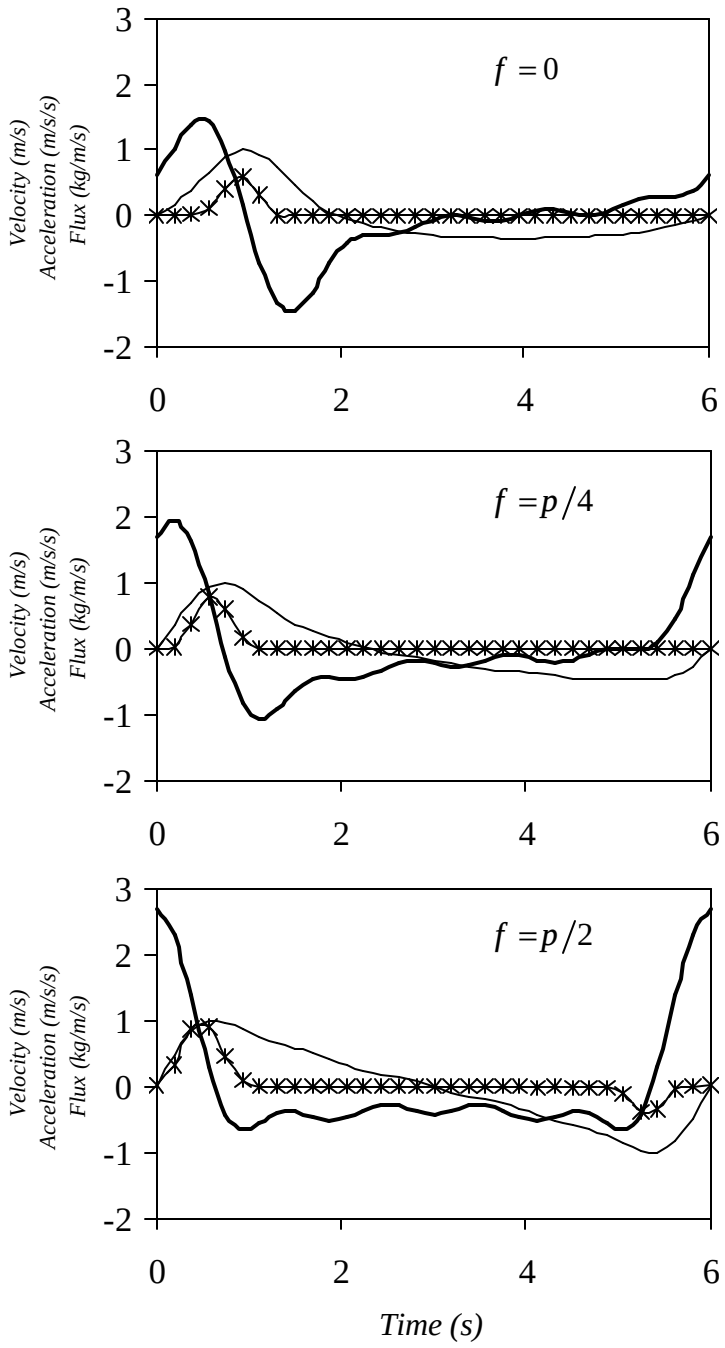

Figure 2.2. Time series of near-bed flow velocity (thin line), flow acceleration (heavy line) and bedload flux (⁎) for transport over a horizontal planar bed for waveform parameter $f = 0$ (top), $f = p/4$ (middle), and $f = p/2$ (bottom).

acceleration and bedload flux for each of the three simulated waveforms is shown in Figure 2.2.

2.3. Energetics-Based Models

Inman and Bagnold [1963] recognized the effect of asymmetrical velocity distributions and presented the following model for the equilibrium beach slope

$$\tan \beta = \tan \phi_r \left(\frac{1-c}{1+c} \right) \tag{2.2}$$

where c is defined as the ratio of the amount of energy dissipated during the offshore sediment flow divided by the amount of energy dissipated during the onshore sediment flow and $\tan \phi_r$ is about 0.63 [*Bagnold*, 1956]. *Bailard and Inman* [1981] refined this relationship to the form

$$\tan \beta = \tan \phi_r \frac{\langle u^3 \rangle}{\langle |u|^3 \rangle} \tag{2.3}$$

where u is the oscillatory flow velocity and angle brackets indicate time averaging. While *Bailard and Inman* [1981] explicitly assume $\tan \beta \ll \tan \phi_r$ in their derivation of equation (2.3), that assumption is often ignored by other workers.

Equation (2.3) predicts β = 25º, 20º and 0º, respectively, for waveform parameter $\phi = 0$, $\pi/4$ and $\pi/2$. Predicted slopes for $\phi = 0$ and $\pi/4$ apparently violate the small-slope assumption; for the sawtooth wave ($\phi = \pi/2$) the time average of any odd moment of the velocity is zero. Finally, the Bailard and Inman prediction of local equilibrium bed slope is independent of grain size.

2.4. Results

Simulations were conducted for a range of bed slopes from –10º to +10º for each of the three waveforms (Figure 2.3). Slopes greater than zero correspond to wave propagation in the uphill direction. Flux for each simulation is time-averaged over one full wave period and has been normalized by the simulated flux for the waveform parameter $f = 0$ at zero slope. The simulation was run for at least two full wave periods and the data from the first period discarded because of transient sorting effects associated with the initiation of a run. The transport rate varies linearly with the tangent of the bed slope, b, for each of the three waveforms for slopes of about –7º to +7º. Only the sawtooth waveform exhibits a local equilibrium beach slope of about 7º; the curves for the other waveforms do not cross the abscissa for the range of slopes simulated to date. For slopes having magnitudes greater than about 7º the dependence of the transport rate on $\tan b$ departs from linearity, and preliminary simulations indicate that the dependence is decidedly nonlinear for slopes having magnitude greater than about 10º. Further simulations are underway to explore this nonlinear dependence.

2.5. Conclusion

The concept of local equilibrium slope for bedload transport processes in the nearshore is difficult to apply in many situations of interest. For example, on beaches composed of coarse sands or gravel, processes of infiltration in the swash zone can drastically alter the gross properties of the onshore- and offshore-directed flows. In this particular case neither energetics-based formulation (equations (2.2) or (2.3)) for the local equilibrium slope is meaningful. Because size-sorting processes are ubiquitous in most

environments having a distribution of sediment sizes, even the grain-size distribution of the bed surface under the onshore-directed portion of the wave period can differ significantly from that under the offshore-directed flow. Perhaps surprisingly, the slope prediction of equation (2.3) is independent of grain size. Our limited results to date strongly suggest that the local equilibrium slope prediction of energetics-based models lacks generality; in particular, it is applicable only to small bed slopes and it predicts zero bed slope for a sawtooth-like waveform common in the nearshore.

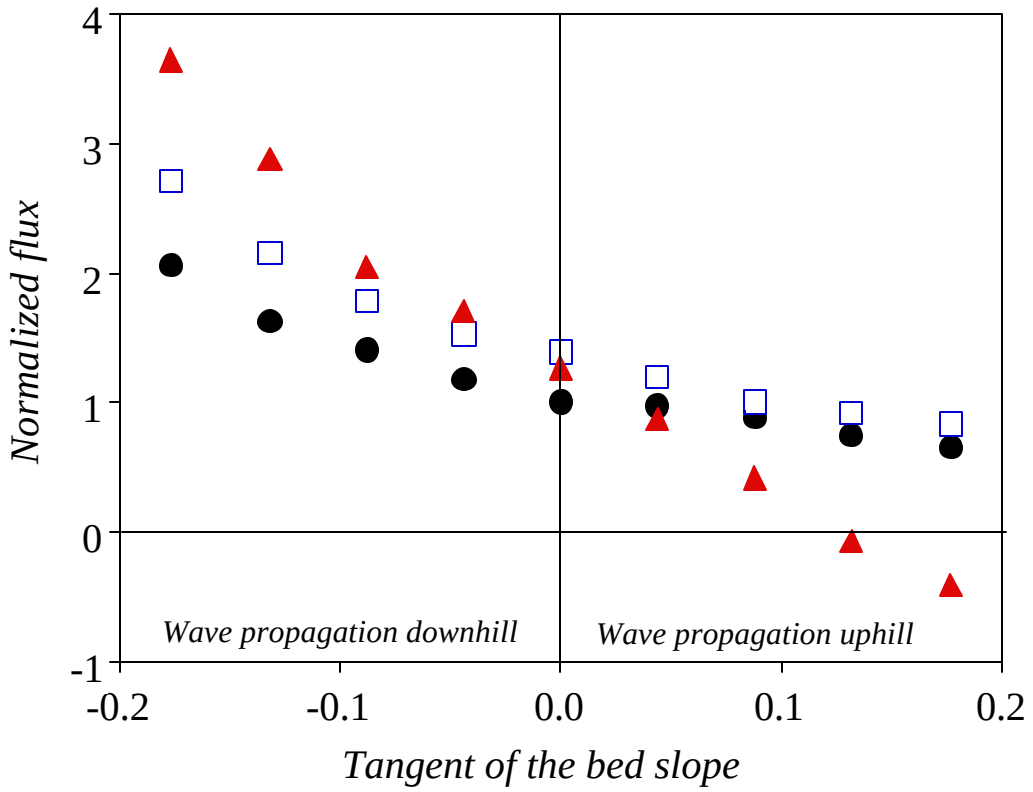

Figure 2.3. Time-averaged net bedload flux versus tangent of the bed slope for three waveforms (closed circle, $f = 0$; open square, $f = p/4$; and closed triangle, $f = p/2$). Each flux is normalized by the flux for $f = 0$ at zero bed slope. A local equilibrium bed slope is evident only for the sawtooth waveform ($f = p/2$) at a bed slope of about 7º.

Chapter 3

Discrete Particle Model for Sheet Flow Sediment Transport in the Nearshore

I co-authored this chapter with Thomas G. Drake and it was published in a slightly different form in the Journal of Geophysical Research, Oceans, volume 106(C9), pages 19,859-19,868, on September 15, 2001.

3.1. Introduction

Particle-scale information necessary to formulate, test, and refine theories for bedload transport and resultant bathymetric evolution in the nearshore is difficult to obtain. Nearshore measurement technologies improved dramatically in the last two decades, yet prevailing models for bedload sediment transport in the nearshore remain essentially untested, except indirectly from measurements of fluid motion and bed elevation. There has been little substantive progress in our understanding of how waves and currents transport sand, especially the high sediment transport rates and concomitant rapid bathymetric evolution associated with storms. Likewise, laboratory observations under field-relevant conditions are rare because relatively few experimental facilities can generate long-period, high-velocity oscillatory flows.

3.1.1. Transport Models

Nearshore bedload transport models are not robust. Energetics models, based on *Bagnold*'s [1966] theory for bedload transport in unidirectional flows, have been extended to unsteady nearshore flows by relating the sediment transport rate to moments of the near-bed fluid velocity [*Bowen*, 1980; *Bailard*, 1981]. Application of the Bagnold/Bowen/Bailard (BBB) models to field measurements predicts storm-generated offshore migration of bars at Duck, North Carolina, with some skill [*Thornton et al.*, 1996; *Gallagher et al.*, 1998]. Fluid motion during storms at Duck is dominated by strong offshore-directed mean currents (although sizable longshore currents are measured in the field, only the cross-shore currents are used in one-dimensional bathymetric models). These currents roughly conform to assumptions used by Bagnold to derive the energetics model. During relatively quiescent conditions, on the other hand, when oscillatory flow velocities are much greater than mean flows, BBB models typically fail to predict gradual onshore bar migration [*Gallagher et al.*, 1998]. We and others have suggested [*Calantoni and Drake*, 1998; *Elgar et al.*, 2001] that transport depends in some measure on the fluid acceleration in addition to fluid velocity. The primary objectives of this study are to indicate the role of fluid accelerations in nearshore bedload transport and to suggest modifications to the BBB models suitable for application to field measurements of nearshore fluid motion. We use discrete particle computer simulations to study the bedload motion of individual sediment particles under a restricted but highly relevant range of nearshore flow conditions: intense, collision-dominated bedload transport of coarse sand grains.

Bagnold's [1966] energetics approach to sediment transport posits that a fraction of the work done by moving fluid on the granular bed is used to transport sediment. A

considerable body of observation and theory support the general form of Bagnold's transport relationship for unidirectional flows. *Bailard*'s [1981] time-averaged bedload sediment flux equation, expressed as mass sediment transport per unit width per unit time (analogous to *Thornton et al.* [1996]), is given as

$$\langle q \rangle = \frac{\rho_s}{g(\rho_s - \rho)} \rho c_f \frac{e_b}{\tan \phi} \left(\left\langle |\mathbf{u}(t)|^2 \tilde{u}(t) \right\rangle + \left\langle |\mathbf{u}(t)|^2 \bar{u} \right\rangle + \frac{\tan \beta}{\tan \phi} \left\langle |\mathbf{u}(t)|^3 \right\rangle \right), \tag{3.1}$$

where q is the bedload flux, ρ and ρ_s are fluid and sediment densities, g is gravitational acceleration, $\mathbf{u}(t)$ is the time-varying velocity, $\tan \beta$ is the bed slope, ϕ is the angle of internal friction, c_f is the friction coefficient, e_b is the bedload efficiency, overbar indicates mean velocity, tilde indicates oscillatory velocity, and angle brackets indicate time averaging. For cross-shore transport of coarse bedload on a horizontal bed due to oscillatory flow, ignoring transport due to mean currents, Bailard's equation reduces to

$$\langle q \rangle = \frac{\rho_s}{g(\rho_s - \rho)} \rho c_f \frac{e_b}{\tan \phi} \left\langle u(t)^3 \right\rangle \tag{3.2}$$

Here we consider a BBB-like model having an additional term depending on an unknown function f of the near-bed fluid acceleration, a:

$$\langle q \rangle = k \left\langle u^3 \right\rangle + f(a) \tag{3.3}$$

Combining all constants in (3.2) into a single parameter k allows us to focus attention on the relative magnitudes of the two terms in (3.3) and to sidestep, for the present, a detailed examination of Bagnold's hypotheses.

3.1.2. Sheet Flow Transport

Large surface gravity waves in shallow water generate intense bedload transport commonly called sheet flow transport [*Dingler and Inman*, 1976], which is thought to be a primary agent in nearshore bathymetric and sedimentologic evolution. Available field [e.g., *Dingler and Inman*, 1976; *Conley and Inman*, 1992] and laboratory [e.g., *Wilson*, 1987; *King*, 1991; *Ribberink and Al-Salem*, 1994; *Sumer et al.*, 1996] observations of sheet flow indicate that bedload motion is confined to a nearly horizontal layer of moving grains up to a few centimeters in thickness with a distinct upper surface. Under sheet flow conditions the bed remains nominally planar and thus roughly corresponds to the upper flow regime in unidirectional flows [e.g., *Gilbert*, 1914; *Middleton and Southard*, 1984]. The absence of ripples and other bed topography during sheet flow simplifies description of the bulk fluid motion to that of a two-phase turbulent flow. *Hanes and Bowen* [1985], *Hanes* [1986], *Nadaoka and Yagi* [1990], and *Jenkins and Hanes* [1992, 1993, 1998] present continuum theories for steady, collision-dominated sediment transport founded on the work of *Bagnold* [1954]. The focus of this paper is on the widely used energetics models and their application to unsteady flows not addressed by the continuum theories.

Descriptions of bedload transport have recently been supplemented by various computer simulation techniques. Discrete particle simulations, originally used in molecular dynamics studies, have been used to address a variety of geophysical applications, including dry granular flows [e.g., *Cundall and Strack*, 1979; *Drake and Walton*, 1995], studies of sea ice ridging [*Hopkins et al.*, 1991] and aeolian sand transport [e.g., *Werner and Haff*, 1988; *Haff and Anderson*, 1993]. *Jiang and Haff* [1993] used discrete particle simulations to study the bedload motion of two-dimensional disks embedded in a discrete fluid. *Schmeeckle*

[1998] used a three-dimensional discrete particle model to address effects of fluid velocity fluctuations in unidirectional flows.

Section 3.2 describes each element of the particle and fluid models employed in the simulations. Section 3.3.3 describes the sensitivity of the model to several parameters. The remainder of the paper describes a comparison of simulation results with several physical experiments and presents a detailed particle-scale picture of oscillatory bedload transport phenomena. Section 3.4.2 proposes a physical mechanism for the inclusion of an acceleration term in the oscillatory bedload transport equation of Bailard and describes a new quasi-empirical formula for sheet flow bedload transport under oscillatory flow that uses fluid motion quantities commonly measured in the field.

3.2. Description of Simulations

In the following discussion the circumstances under which the simulations provide a reasonable description of the physical processes and where they do not are distinguished, insofar as available physical observations permit comparison. Much emphasis has been placed on studying the initiation and subsequent motion of bedload particles when the interface between fluid and bed is well defined and the transport rate is small. The usual conceptual approach in these studies starts with a description of the motion of the fluid above the granular bed and calculates the resulting particle motion [e.g., *Wiberg and Smith*, 1985; *Sekine and Kikkawa*, 1992; *Niño and Garcia*, 1994, 1996]. Under these conditions, interaction between bedload particles can be neglected, as can the effects of moving particles on the bulk fluid motion. The conceptual approach adopted herein starts with some knowledge of the clearly immobile grains in the bed and then describes the individual and

collective particle motion that occurs when fluid stresses exceed the shear strength of the granular bed. The approach explicitly de-emphasizes the short initial and final stages of grain motion over a relatively immobile bed and hypothesizes that grain-grain interactions dominate the stresses within a high-concentration granular fluid. Such interactions begin to dominate over fluid interactions when the solids volume concentration exceeds about 8% [*Bagnold*, 1954].

One commonly used measure of the relative importance of interstitial fluid effects in grain-fluid systems is the Bagnold number [e.g., *Hanes and Bowen*, 1985]

$$B = \rho_s D^2 \lambda^{\frac{1}{2}} \frac{du}{dz} \mu^{-1} \tag{3.4}$$

where D is the grain diameter, du/dz is the velocity gradient, μ is the dynamic fluid viscosity, and the linear concentration λ [*Bagnold*, 1954] is

$$\lambda^{-1} = (N_0/N)^{\frac{1}{3}} - 1 \tag{3.5}$$

where $N_0 \approx 0.65$ is the maximum value of the solids volume concentration N. For values of $B \geq 450$, Bagnold's experiments indicate that grain-grain interactions dominate viscous effects. The simulations presented here address such collision-dominated granular fluid flows.

Using *Dingler and Inman*'s [1976] field criterion for incipient sheet flow,

$$\Theta = \frac{\rho U_{\max}^2}{(\rho_s - \rho) g D} \geq 240, \tag{3.6}$$

maximum orbital velocities $U_{\max}$ on the order of 1 m s^{-1} are required to induce collision-dominated sheet flow of coarse quartz sand in water if both $\Theta \geq 240$ and $B \geq 450$ are to be satisfied. Assuming that particle-particle interactions dominate momentum transfer greatly

simplifies the treatment of particle-fluid interactions because it justifies neglecting lubrication forces between particles.

In the discrete particle model, velocities and positions of discrete spherical particles are obtained by integrating Newton's equations of motion at small time steps, and an analogous set of equations for the torques on the spheres is solved to provide their spins and orientations. Forces are generated by direct particle-particle contact; by such fluid-particle interactions as buoyancy, drag, and added mass effects; and by pressure gradients and gravitational forces. An eddy-viscosity-based model describing interactions between discrete fluid elements completes a self-consistent physical description of the bedload transport process.

3.2.1. Particle-Particle Interactions

Normal and tangential forces between contacting spheres are based on approximations [*Walton and Braun*, 1986*a*, 1986*b*; *Drake and Walton*, 1995] to theoretical models for identical, homogeneous Hertzian elastic spheres developed by *Mindlin and Deresiewicz* [1953]. The magnitude of the normal force F_n between contacting particles is given by

For loading (approaching particles)

$$F_n = k_1 a \tag{3.7}$$

For unloading (receding particles)

$$F_n = \max[k_2 (a - a_0), k_3 a] \tag{3.8}$$

where a is the overlap of particles, a_0 is the value of a where the unloading curve goes to zero, and k_1, k_2, and k_3 are constants. No negative values are allowed for F_n. For binary collisions the coefficient of normal restitution e is approximately

$$e = (k_1/k_2)^{\frac{1}{2}} \tag{3.9}$$

The tangential force F_t, described in detail by *Drake and Walton* [1995], is

$$F_t = \min(|k_t ds|, |m_f F_n|), \tag{3.10}$$

where k_t is the tangential stiffness, *ds* is the tangential displacement at the contact point, m_f is the friction coefficient (no distinction is made here between sliding and static friction), and the sign of F_t opposes relative motion of the spheres at the point of contact.

The particular models used here were tested and refined by comparisons of simulations with physical experiments of dry granular flows using homogeneous plastic spheres [*Drake and Walton*, 1995; *Foerster et al*., 1994]. Bedload transport simulations using the same plastic spheres compare favorably with physical experiments [*Drake et al.*, 1991] and are insensitive to variations in the particle stiffnesses and friction coefficient, a feature also noted by *Jiang and Haff* [1993]. Interparticle force models used in discrete particle simulations are the subject of considerable research. A discussion of potential pitfalls (primarily associated with velocity-dependent damping models not used here) is given by *Luding et al.* [1994]. Natural sand and gravel particles are neither spherical nor homogeneous, and whereas our simulations are robust with respect to the details of particle-particle interactions, we are also pursuing studies of nonspherical, inhomogeneous particles (see Chapter 5) that may explain subtle features of the simulations noted in section 3.3.

3.2.2. Discrete Fluid Model

A crude discrete fluid model drives bedload transport in the simulation (Figure 3.1). Pressure-gradient forces generated by the progression of an idealized surface gravity wave accelerate a stack of thin horizontal layers of fluid and the spherical particles embedded

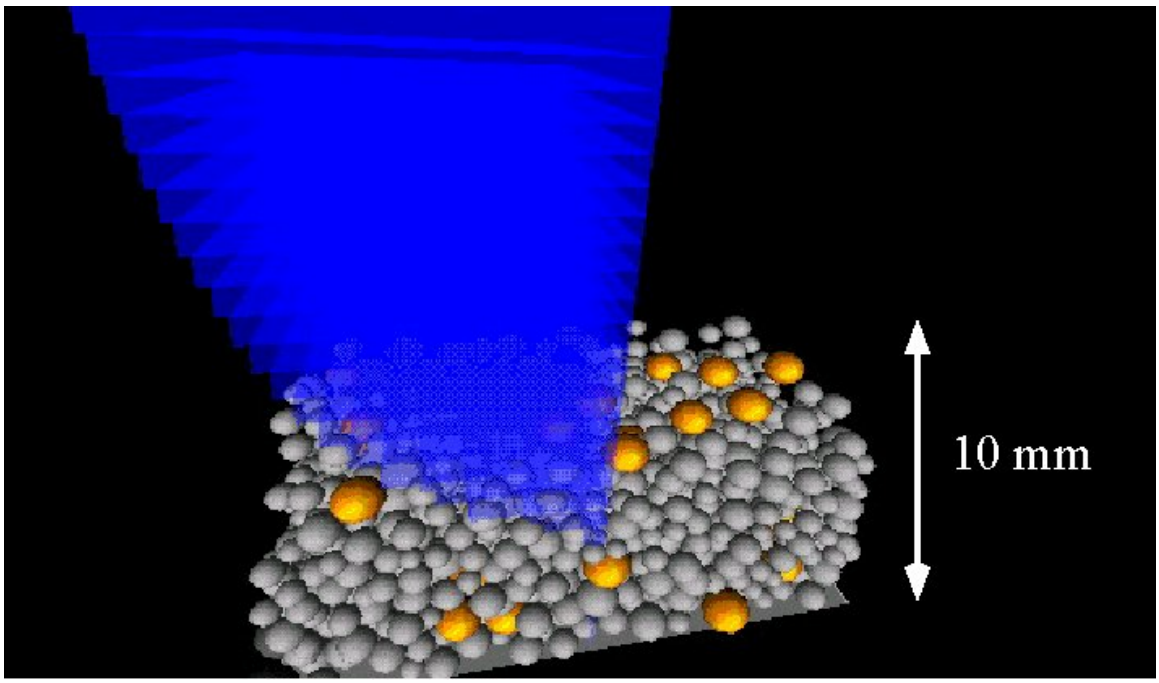

Figure 3.1. Schematic picture of discrete particle simulation. Sand grains are modeled as frictional spheres having the density of quartz ($r = 2650$ kg m^{-3}) and a distribution of sizes corresponding to experiments by *King* [1991]. Grains larger than 1.5 mm diameter are colored gold to aid visualization of particle sorting processes. Fluid motion is modeled using discrete slabs constrained to move parallel to the bed. Length of the slabs is proportional to fluid velocity. Periodic boundaries are used in both the cross-shore and alongshore directions; large grains are fixed to a smooth basal plane to prevent bulk sliding of the granular assemblage.

within them. Linear wave theory is used to determine the fluid pressure gradients at the bed [*Guza and Thornton*, 1980]. Streamwise fluid pressure gradients within the volume are approximately constant because the dimensions of the simulation volume are small and thus closely resemble those in a laboratory flow tunnel. The layers in the stack exchange momentum via an eddy viscosity determined from a mixing length model. Each fluid layer exerts drag, added mass, and pressure gradient forces on particles embedded within it. Particles exert equal and opposite forces on the fluid layers, thus fully coupling fluid and sediment motion. Turbulence is implicit in a mixing length approach, and thus the fluid velocity within each layer is constant and explicitly excludes particle-generated wakes or other grain-scale turbulent fluid motions. The layer model inherently suppresses development of such bed features as ripples. However, under sheet flow conditions, local bed topography is planar.

The choice of mixing length model is largely guided by the desire to minimize simulation complexity and is an area for improvement. A mixing length model provides a simple mechanistic picture of the fluid-grain mixing process, despite its well-known limitations [e.g., *Tennekes and Lumley*, 1972]. The effective viscosity ν_{eff} that mediates momentum transport between fluid layers is the maximum of the fluid kinematic viscosity ν and an eddy viscosity:

$$\nu_{eff} = \max\left(\nu, \; \rho l^2 \left|\frac{\partial u}{\partial z}\right|\right), \tag{3.11}$$

where l is the mixing length. The mixing length is the vertical distance upward from an origin z_0 taken where the volume concentration of particles N_z exceeds a fixed value, typically 0.4 (specification of N_z in the simulations is discussed in more detail in Section

3.3.3.3). Defining the origin of the mixing length is problematic, as the problem is not only geometrical. For example, the nominal bed level defined by fluid flow considerations, such as the origin of a logarithmic velocity profile, is not necessarily the same as that defined by particle motion considerations, such as the average elevation of the tops of surface particles [*Drake et al.*, 1988].

The mixing length model enforces a law-of-the-wall velocity profile, except in the region of bedload motion and immediately above it, where momentum extracted by particles causes significant deviations from a particle-free velocity profile. Exploratory simulations using alternative forms for the effective viscosity [e.g., *Trowbridge and Madsen*, 1984*a*, 1984*b*] proved insensitive to the choice of model.

3.2.3. Particle Fluid Interactions

The equation of motion for sediment particles [*Madsen*, 1991] is

$$\rho_s V \frac{d\mathbf{u}_s}{dt} = (\rho_s - \rho) g V + \rho V \frac{D\mathbf{u}_f}{Dt} + c_m \rho V \left(\frac{D\mathbf{u}_f}{Dt} - \frac{d\mathbf{u}_s}{dt} \right)$$

$$+ \tfrac{1}{2} \rho C_d A \left| \mathbf{u}_f - \mathbf{u}_s \right| \left(\mathbf{u}_f - \mathbf{u}_s \right) + \mathbf{F}_f \,, \qquad (3.12)$$

where $\mathbf{u}_s$ and $\mathbf{u}_f$ are the sediment and fluid velocities, V and A are the volume and projected area, respectively, of the sediment grain, C_d and c_m are the drag and added mass coefficients, and $\mathbf{F}_f$ represents intergranular forces. Neither lift forces nor so-called Magnus forces arising from particle rotation are included. Lift forces are neglected because vertical gradients in bed-parallel fluid velocity within the sheet flow layer are small (H. Seltmann and T. G. Drake, unpublished laboratory data, 1996). Other investigators, most recently *Schmeeckle* [1998], have measured significant lift forces in the vicinity of fixed grains in unidirectional

flows. However, the turbulent structure in such fully developed boundary layer flows differs significantly from that in oscillatory boundary layers. Finally, although particle rotations are generated by frictional particle contacts, no fluid drag forces resist rotational motion in the simulation.

The first four terms on the right-hand side of (3.12) represent the buoyancy force, the fluid acceleration force, the added mass force, and the drag force. *Jiang and Haff* [1993], following *Landau and Lifshitz* [1987], accounted for the added mass force by increasing the particle mass by 20%, appropriate for quartz-density particles in water. Here the coefficient of added mass, c_m, is 0.5 [*Batchelor*, 1967]. The drag coefficient C_d depends on the instantaneous value of the particle Reynolds number $Re_s = U_{rel} D/u$ as follows:

$$C_d = 24 Re_s^{-1} + 4 Re_s^{-\frac{1}{2}} + 0.4 , \tag{3.13}$$

where U_{rel} is the magnitude of the relative velocity between sediment and fluid. Experiments to determine C_d for fixed grains in a steady, uniform unidirectional flow by *Schmeeckle* [1998] indicate that the still water coefficient described by (3.13) underestimates the true drag coefficient by as much as 50% or more. Engineering studies of fluidized bed phenomena indicate that both c_m and C_d may depend strongly on local volume concentration [e.g., *Allen*, 1980; *Richardson and Meikle*, 1961; *Rowe and Henwood*, 1961]. However, qualitative features of the simulations are unaffected by the simplifications adopted here, and the relatively small variations in such quantitative measures as mean sediment transport rate arising from the use of more complicated expressions fail to justify their use until further studies indicate otherwise.

3.3. Sheet Flow Simulations

Simulations of oscillatory sheet flow are compared with the limited data available from physical experiments. Additional simulations explore a small subset of the parameter space to determine simulation sensitivity to variations in parameters, particularly those that are poorly constrained by theory or observation. A final set of simulations explores waveform effects and critically tests BBB models with the results used to propose an additional term for the BBB equations.

3.3.1. Description of Simulations

Figure 3.1 is a schematic diagram of the simulations. Periodic boundaries are used in both the cross-shore and alongshore directions, and thus particles exiting any side of the calculational volume are reintroduced with identical velocity and rotation at the opposite side of the volume. The lower boundary of the calculational volume is a smooth plane to which several spheres are fixed to prevent wholesale sliding of the granular assemblage, and the thickness of the granular bed is chosen such that the maximum depth of motion never reaches the fixed bed spheres. The initial particle configuration for each simulation is generated by gravitational settling of particles from a regular lattice into the calculational volume. Although larger particles settle more rapidly than smaller ones, the relatively high concentration effectively hinders size sorting during the settling process.

3.3.2. Comparison With Experiment

Few experiments satisfying the Bagnold number (equation (3.4)) and incipient sheet flow (equation (3.6)) criteria exist for comparison with simulations. The primary experimental difficulty is generating a many grains thick bedload layer of large, dense

particles. *King*'s [1991] flow tunnel experiments using 1.1-mm mean diameter quartz sand (Figure 3.2) provide sediment transport rates for half-cycle oscillatory flows under sinuosoidal and other waveforms in both horizontal and tilted bed configurations. Although King's data do not include all the information necessary to calculate the Bagnold number, conservative estimates of the quantities in (3.4) for a number of King's experimental runs greatly exceed Bagnold's criterion, except at the initiation and cessation of motion. Simulated transport rates for half-period sine waves having periods and maximum fluid velocities identical to King's experiments are compared in Figure 3.3. For maximum fluid velocities <1.1 m s^{-1} the simulated rates are within 20% of King's measured rates. For maximum fluid velocities >1.1 m s^{-1}, agreement is within 25%. Simulation transport rates are mean rates calculated from at least three half periods, and transport rates during the first half period of a simulation are excluded due to transient size sorting of the initial particle configuration.

3.3.3. Simulation Sensitivity to Parameter Variation

Several parameters must be specified for simulation of sheet flow, including several describing properties of solid particles and discrete fluid layers. This section discusses simulation sensitivity to these parameters and physical reasoning for specifying parameters that are poorly constrained by theory and/or physical experiment.

3.3.3.1. Particle Parameters

Natural sediment comprises rough, inhomogeneous particles having a wide range of sizes and shapes. In some environments (not considered here), sediment density can also vary appreciably. Spherical sediment grains used in the simulations can be tractably described with a minimum of parameters, including particle stiffness, coefficient of normal restitution,

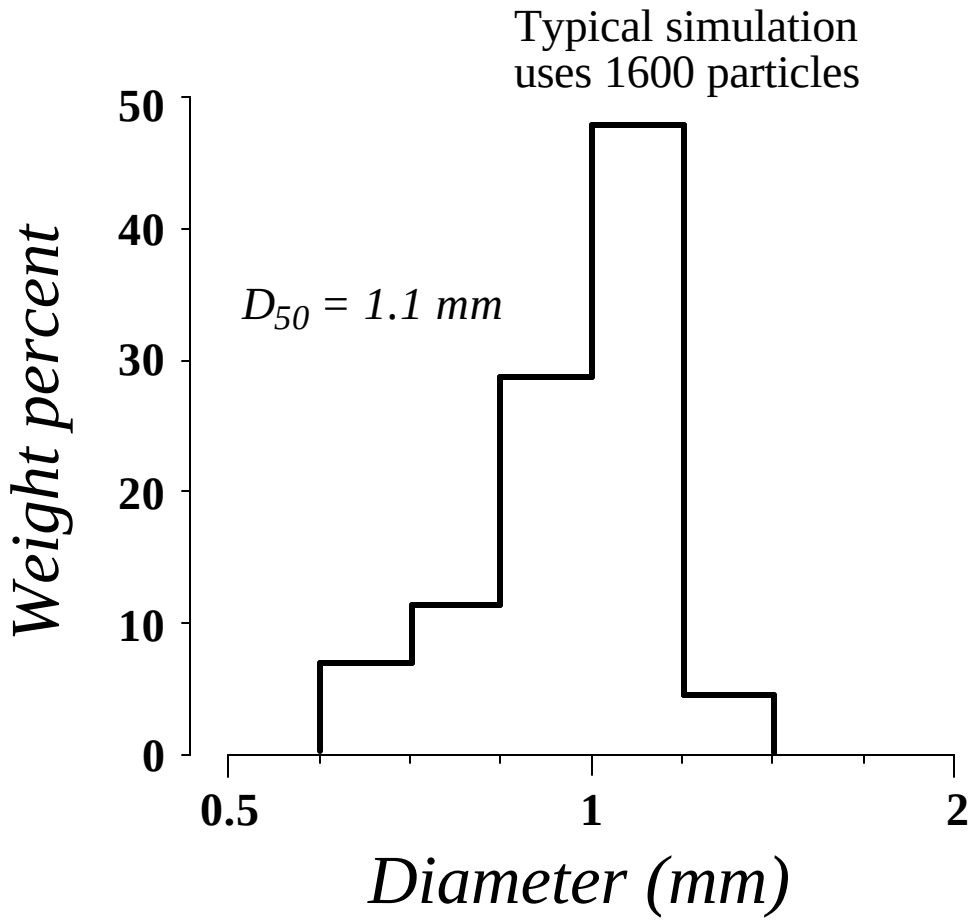

Figure 3.2. Grain-size distribution for *King* [1991] flow tunnel experiments sharply peaked about a mean grain size of 1.1 mm.

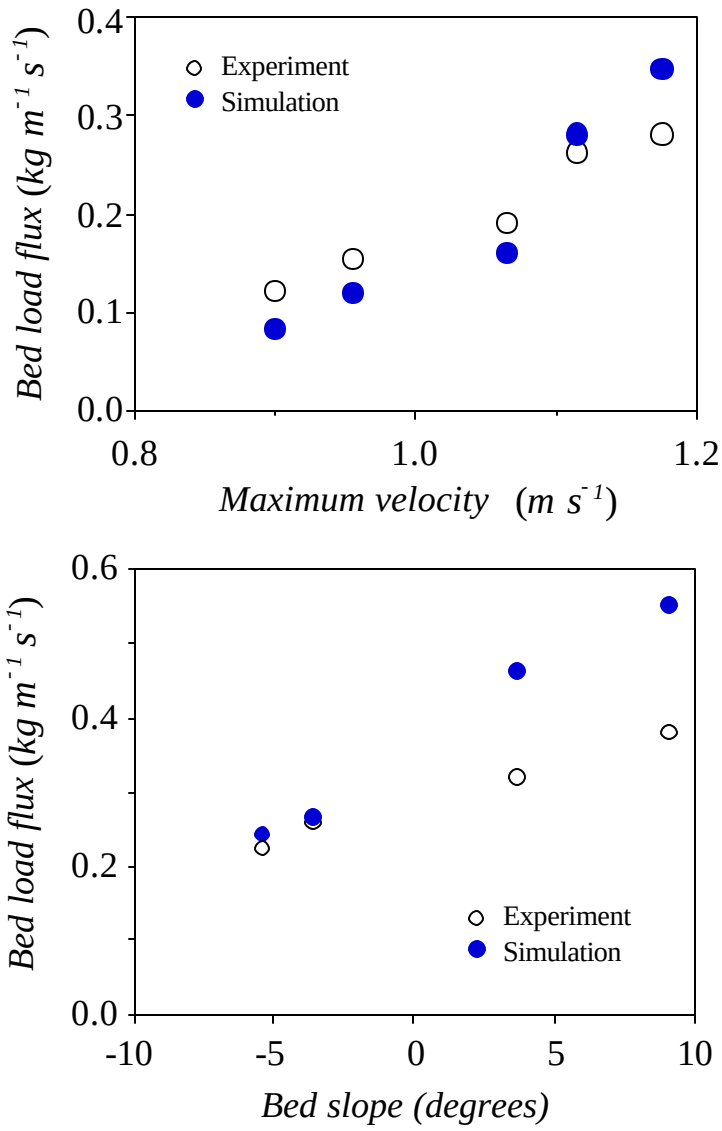

Figure 3.3. Comparison of predicted bedload transport rates from simulations with physical experiments conducted by *King* [1991] in an oscillatory flow tunnel using natural quartz sand with the distribution of sizes shown in Figure 3.2. (top) Bedload flux produced by maximum free stream fluid velocities ranging from just above that required for incipient motion to nearly 1.2 m s^{-1}. (bottom) Bedload flux versus bed slope for maximum free stream fluid velocity of 1 m s^{-1}.

and friction coefficient, several of which were varied while holding others fixed. While the initiation and cessation of sediment motion may be described only poorly in simulations using spherical particles, physical experiments [*Drake et al.*, 1991] imply that the bulk properties of a thick bedload layer are largely independent of particle shape. Description of the parameters and simulation sensitivity to parameter variations are reported below. Although some of the parameters for natural sediments are poorly known, sensitivities are small. We define baseline simulations as those simulations in which the stiffness $k_1 = 10^5$ N m^{-1}, the normal coefficient of restitution e = 0.6, and the coefficient of friction $m = 1$.

Particle Stiffness.

The stiffness of pure quartz spheres can be calculated from elastic constants, but stiffness measurements for individual clasts in natural sediments comprising single mineral grains or aggregates of them are exceedingly difficult. Thus the stiffness k_1 in discrete particle simulations is essentially a free parameter, constrained by physical and pragmatic computational concerns. Small values of the stiffness promote excessive overlap at particle contacts and increase the contact duration and thus are unsuited, for example, to simulations of acoustic wave propagation. In dispersed, fluid-free, collision-dominated flows the stiffness can be reduced by several orders of magnitude, thus decreasing the fixed computation time step significantly with negligible effect on flow dynamics [*Drake and Walton*, 1995]. In bedload transport over loose beds, however, both brief collisions and enduring static contacts between grains are important. In the present simulations the stiffness was varied over several orders of magnitude with negligible effect on such bulk quantities as sediment transport rate. In no case was the overlap of contacting particles allowed to exceed 1% of a particle

diameter, and typical overlaps were much less than 0.5%. The duration dt of a particle-particle collision in the absence of fluid forces is proportional to the normal coefficient of restitution, e, and inversely proportional to $k_1^{1/2}$. In practice, dt was typically $\sim 4\times10^{-4}$s in the simulations, using $k_1 = 10^5$ N m^{-1}.

Restitution Coefficient.

The normal coefficient of restitution for irregular natural particles varies considerably depending on the particle and collision geometries. Tabletop experiments (T. G. Drake, unpublished data, 1996) using natural sand and gravel particles indicate a range of e from >0.8 to <0.1, typically in the range 0.1 to 0.5. Recent experiments by *Schmeeckle* [1998] also indicate coefficients of restitution for immersed particle collisions in a similar range. Bedload transport rates in the simulations are insensitive to the restitution coefficient. Differences in instantaneous transport rates for e=0.15, 0.3, and 0.6 are statistically insignificant. Baseline simulations use e=0.6.

Friction Coefficient.

Sensitivity to variations in friction coefficient m is small, provided that m is nonzero. The presence of surface asperities on natural rough particles typically prevents relative tangential velocity at particle contacts, and adopting $m \geq 1$ for geometrically smooth spheres effectively approximates the observed rotational motion of natural particles [e.g., *Drake et al.*, 1988]. Baseline simulations use $m = 1$.

3.3.3.2. Fluid Layer Parameters

Typical simulations used at least 40 fluid layers having a minimum thickness greater than or equal to D_{50} (D_x indicates that x% by weight of the particles had diameters smaller

than D_x). Simulations are insensitive to the number of fluid layers, provided that at least some layers always remain grain-free during the simulation. Layer thickness was chosen to resolve sufficient particle-scale detail in the bedload layers and to minimize statistical uncertainties in simulation quantities. In particular, layers thinner than the mean particle diameter often have too few particles for statisically significant determination of layer concentration. In contrast, simulations using fluid layers thicker than about one or two mean particle diameters often exhibit discontinuities in transport rates and also grossly mispredict initiation of particle motion. In practice, the typical layer thickness was 1 mm, which also ensured that each particle occupies volume in, at most, two layers.

3.3.3.3. Nominal Bed Concentration

The free parameter N_z is symptomatic of the uneasy but requisite union of granular and fluid mechanics at the sediment-water interface. The choice of $N_z = 0.4$ is justified heuristically as follows. At concentrations exceeding 0.4 the mean free path between particles is less than half a particle in diameter and vertical exchange of grains within the sheet flow layer is diminished greatly. Bulk transport of fluid momentum by eddies is likewise inhibited and is effectively limited to scales larger than the thickness of the discretized fluid layers. Perhaps surprisingly, the simulations are rather insensitive to variations in N_z (Figure 3.4).

3.3.3.4. Effect of Computational Domain Size

Computational domain size has both scientific and practical implications for discrete particle simulations, which use periodic boundaries to minimize the number of simulation particles and, in turn, the computational resources. *Drake and Walton* [1995] extensively tested a discrete particle simulation for dry granular flows and found such bulk flow

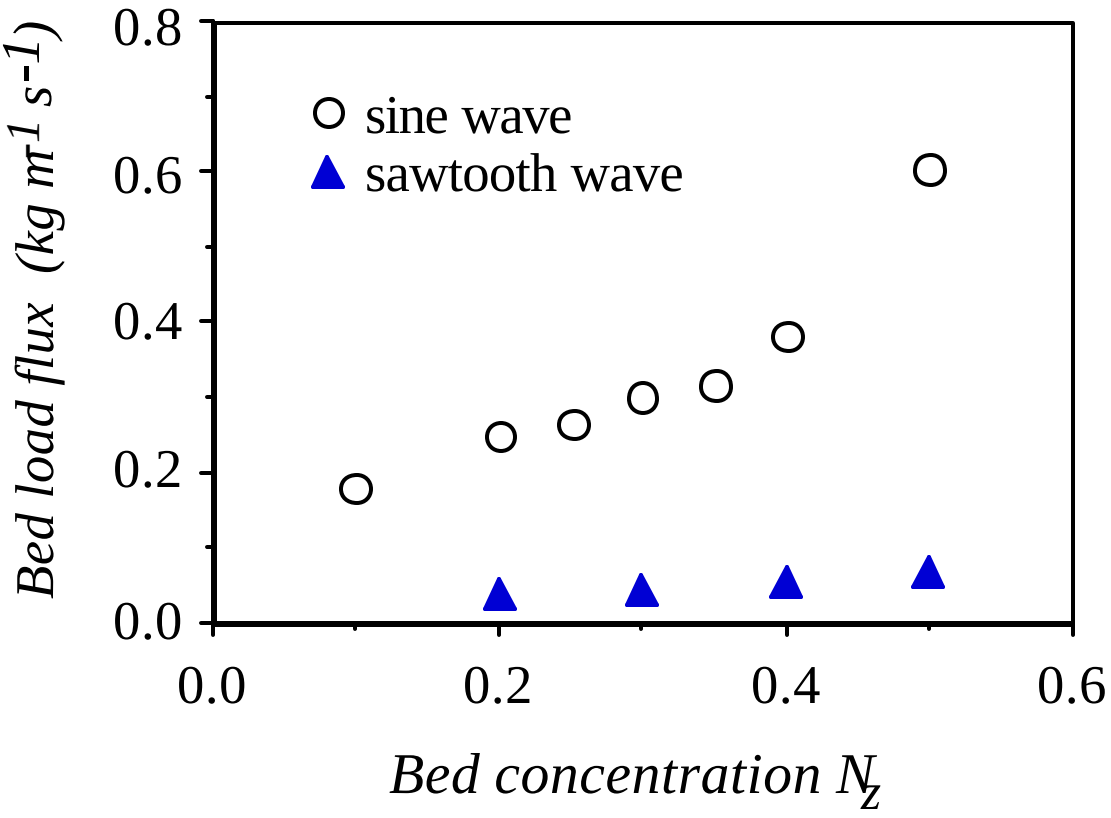

Figure 3.4. Time-averaged bedload transport rate, weakly dependent on the bed concentration N_z, which fixes the origin for determination of the mixing length. Circles indicate variation of N_z for one half-period (i.e., onshore) sinusoidal oscillatory flow having a period of 6 s and maximum free stream velocity of 1 m s^{-1}. Triangles indicate variation in net flux for a full 6-s period sawtooth oscillatory flow having the same maximum free stream velocity of 1 m s^{-1}. Weak dependence of transport rate on N_z for $0.2 < N_z < 0.5$ is observed for all simulated flows.

descriptors as transport rate to be largely insensitive to variations in computational domain size, provided the domain exceeded certain minimum dimensions. Similiar testing of the present simulation indicates that a cross-stream domain dimension of only about five particle diameters is sufficient. The height or thickness of the computational domain should be at least twice the thickness of the bedload layer, with a streamwise domain dimension roughly equal to the domain height. Dependence of transport rates on domain dimensions is small; a worst-case disparity of 13% increase in transport rate occurred in a simulation for which the streamwise domain dimension was doubled from the baseline value. Such variability is small relative to natural fluctuations in transport rates and fluid forcing.

3.3.3.5. Computational Issues

Computational resources presently limit the number of particles in the simulations to a few tens of thousands of spheres. Computing schemes using massively parallel hardware might increase the number of particles by 2 orders of magnitude or more, but the length scales of such systems would still be exceptionally small relative to the typical scales of interest in nearshore processes. Using highly vectorized and parallelized Fortran code on an (now obsolete) eight-processor Cray Y-MP, for example, the simulations attain an average performance of just over 1 GFlop when operating in parallel. We used nominally identical code on a number of computing platforms and found only very small numerical differences between simulations on different hardware. We attribute such differences to the order in which vector additions are performed by vector processors and to internal representation of numbers; such differences are insignificant at any level of physical relevance.

3.4. Simulation of Surf Zone Conditions

3.4.1. Simulated Waveforms

A suite of simulations using five different waveforms having a constant period T=6 s and maximum fluid velocities of 0.5, 0.75, 1.0, 1.25, and 1.5 m s^{-1} was used to explore the effects of wave shape on bedload transport. As expected, simulated waveforms producing 0.5 m s^{-1} maximum fluid velocities transport essentially no sediment. The time-varying pressure gradient force $F(t)$ exerted on the slabs and grains in the stack is proportional to

$$F(t) \propto \sum_{i=0}^{4} \frac{1}{2^i} \sin\left[(i+1)wt + if\right] \tag{3.14}$$

where $w = 2p/T$ and f is the waveform parameter. The waveform parameter corresponds to the biphase [e.g., *Elgar and Guza*, 1986; *Elgar and Chandran*, 1993]. Figure 3.5 shows near-bed fluid velocity time series for waveforms having $f = 0$, $p/4$, and $p/2$ (waveforms having $f = p/8$ and $3p/8$ were also simulated). Such variation in f encompasses a wide qualitative range of shoaling and broken waves. We also simulated waveforms having $f > p/2$, but such waves are not typical of natural surf zones. They can, however, be produced in the laboratory and thus offer opportunity for future testing of the generality of our simulation results.

3.4.2. Role of Acceleration in Unsteady Bedload Transport

Bedload transport rates for some simulated waveforms are described poorly by the BBB energetics models, which depend only on odd moments of the fluid velocity. In particular, for sawtooth waveforms typical of broken waves in the surf zone ($f = p/2$), net

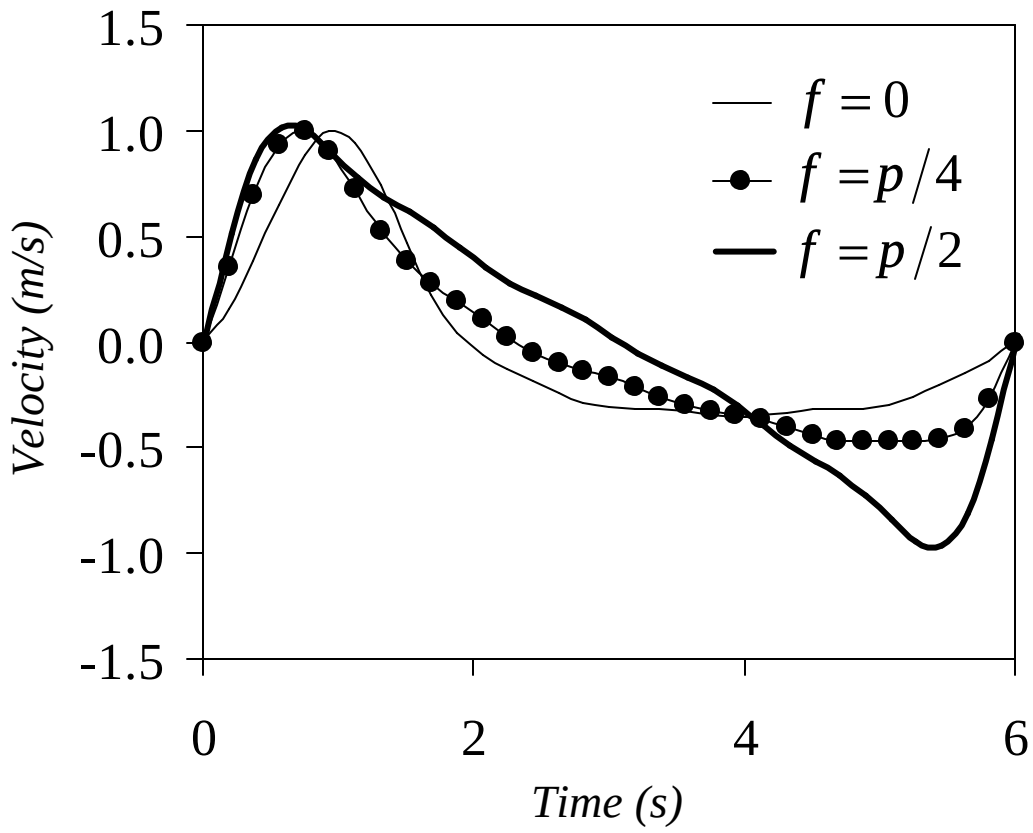

Figure 3.5. Variation in waveform for $f = 0$, $p/4$, and $p/2$ for 6-s wave periods having a maximum fluid velocity of 1 m s^{-1}. Increasing f corresponds to waveform evolution due to shoaling and breaking. The sawtooth waveform corresponding to $f = p/2$ is characteristic of surf zone bores. Waveforms for $f = p/8$ and $3p/8$ are not shown.

transport rates from the simulation are large and onshore directed. For such sawtooth waveforms, odd moments of the velocity are zero, and thus the BBB models predict no transport. Intense bedload transport occurs during only a small fraction of the wave period and is correlated strongly with spikes in the fluid acceleration (Figure 3.6). Substantial transport in these simulations is described better by a measure of the fluid acceleration; the magnitude of such accelerations in the nearshore can be considerable. *Elgar et al.* [1988] inferred fluid accelerations up to 300 cm s^{-2} from velocity measurements under 1-m-high broken waves. Such accelerations are roughly analogous to tilting the bed surface 20º from the horizontal. We now outline an approach to modification of the existing BBB models to incorporate acceleration effects.

Spikes in the forcing function (equation (3.14)) acting on the boundary layer can be treated as impulses that transfer momentum to the near-bed fluid and sediment. The impulse I is defined as

$$I = \int_{t_{initial}}^{t_{final}} F(t)dt \ , \tag{3.15}$$

where F is the pressure gradient force exerted on the granular fluid mixture by the passage of a wave. The total impulse-generated bedload transport, Q, where

$$Q = K_a I \tag{3.16}$$

and K_a is a constant, is directly proportional to the impulse (Figure 3.7). The impulse can be calculated directly from the simulation, but the challenge is to find a suitable proxy for the impulse-induced sediment transport that circumvents the need to determine the limits of integration in (3.15) from field data. Even if high temporal resolution time series of near-bed velocity are available, a straightforward methodology to determine integration limits for

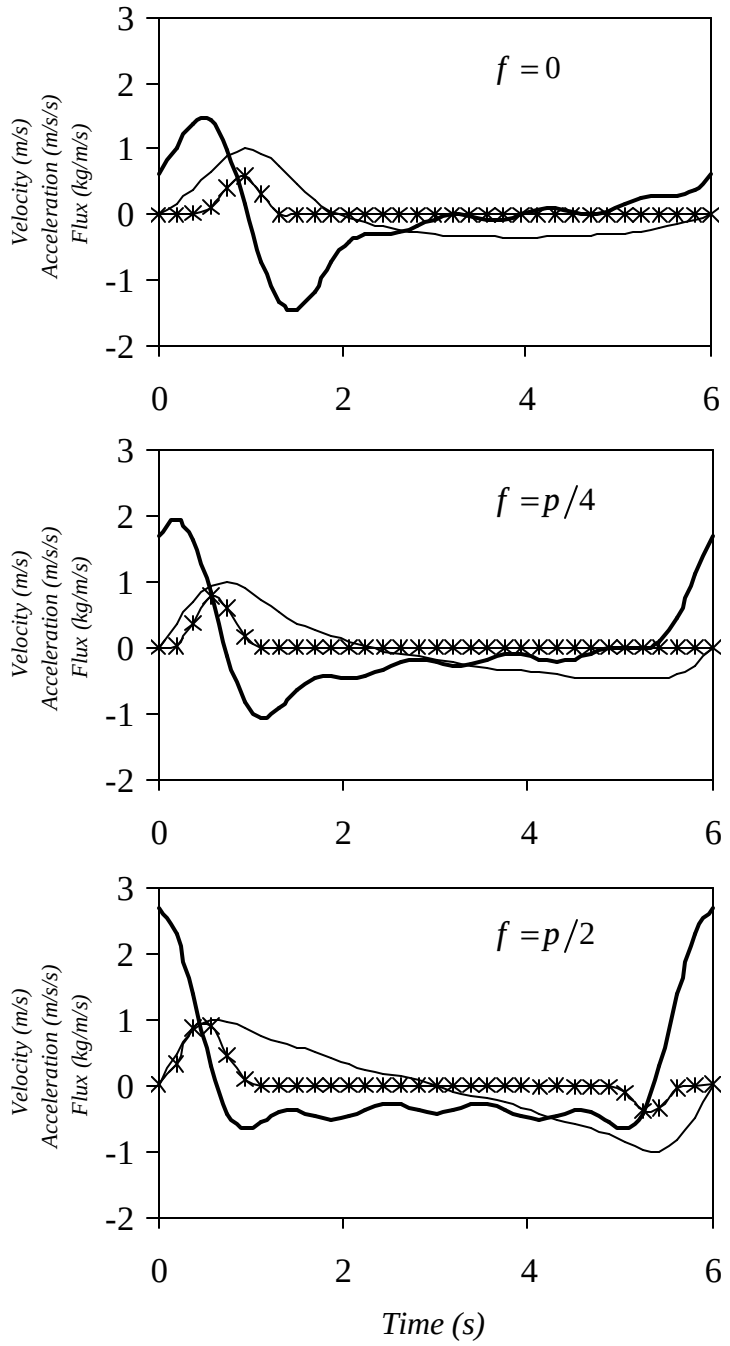

Figure 3.6. Time series of near-bed fluid velocity (thin line), acceleration (thick line) and bedload flux (circles) from simulated waveforms having $f = 0$, $p/4$, and $p/2$. Wave period is 6 s and maximum fluid velocity is 1 m s^{-1} for each simulation. Net bedload transport in all cases is onshore directed. Offshore-directed transport occurs only under the sawtooth waveform ($f = 0$). Episodic, intense, onshore-directed transport occurs when velocity and acceleration have the same sign (direction).

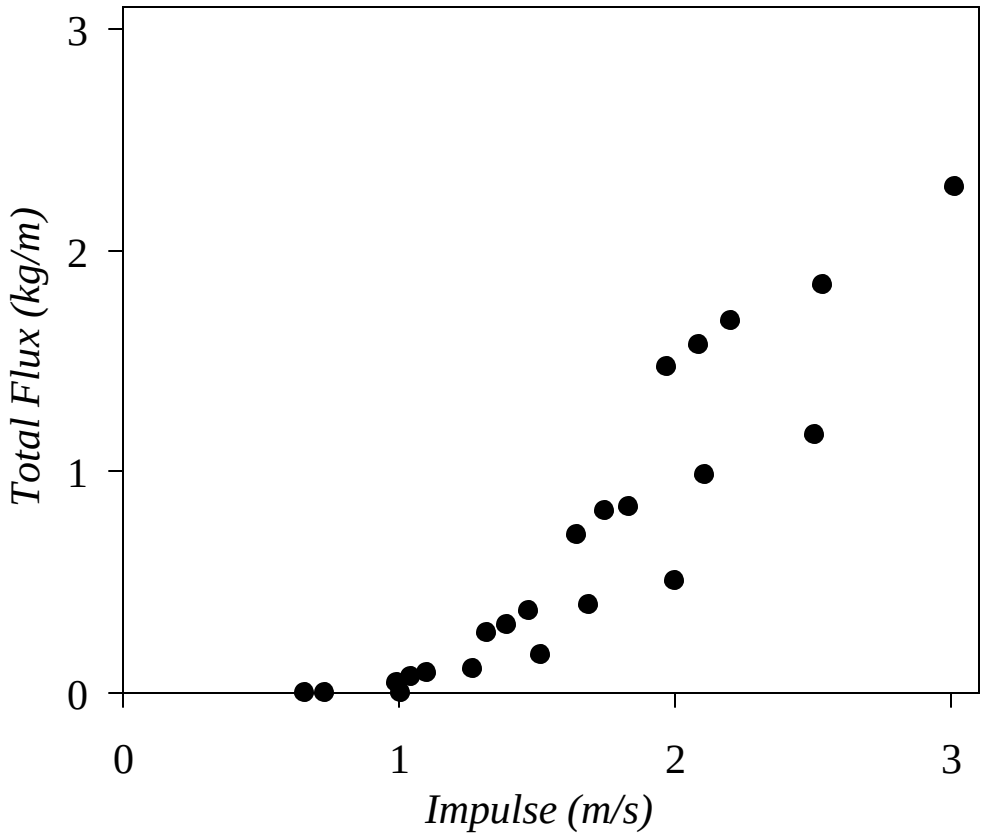

Figure 3.7. Total impulse-generated transport, increasing linearly with impulse above a minimum impulse of ~1 m s^{-1}. The impulse is obtained by integrating the acceleration versus time curve with limits of integration corresponding to zero crossings of the fluid acceleration. Total transport is the integral of the entire flux versus time curve.

(3.15) is lacking. Instead, we propose the use of a fluid-motion descriptor, a_{spike}, easily calculated from velocity measurements commonly obtained in field experiments and defined as follows:

$$a_{spike} = \langle a^3 \rangle / \langle a^2 \rangle, \tag{3.17}$$

where a is the magnitude of the fluid acceleration. The modified BBB equation (3.3) becomes

$$\langle q \rangle = \begin{cases} k \langle u^3 \rangle + K_a (a_{spike} - a_{crit}), & a_{spike} \geq a_{crit} \\ k \langle u^3 \rangle, & a_{spike} < a_{crit}, \end{cases} \tag{3.18}$$

where a_{crit} is the critical value of a_{spike} that must be exceeded before acceleration enhances transport. Linear regression of our data (Figure 3.8) suggests $K_a = 0.07 \text{kg s m}^{-2}$ and $a_{crit} \approx 1 \text{ m s}^{-2}$. Alternatively, the transport relationship in (3.18) can be cast in terms of the non-dimensional acceleration skewness [*Elgar*, 1987; *Elgar et al.*, 2001] with a suitable scaling factor. Our definition of a_{spike} incorporates one possible choice of scaling: $a_{spike} = \langle a^2 \rangle^{1/2} a_{skew}$; future work may suggest other formulations.

Perhaps surprisingly, the best fit value of k from the BBB models is $0.8 \text{ kg s}^2 \text{ m}^{-4}$, or ~ 6 times greater than that suggested by use of common parameter values in the BBB models. In those models,

$$k = \frac{r_s}{g(r_s - r)} r c_f \frac{e_b}{\tan f}. \tag{3.19}$$

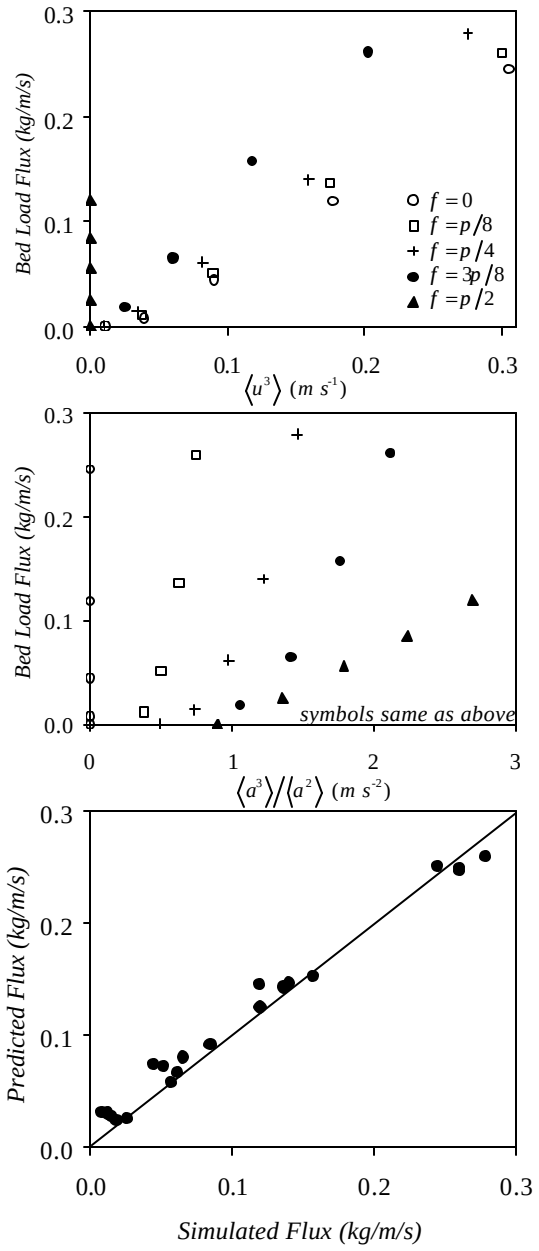

Figure 3.8. (top) Bedload flux varying approximately linearly with $\langle u^3 \rangle$, except for strongly asymmetric waves having $f = p/2$ and $\langle u^3 \rangle$ equal to zero. (middle) Variation in bedload flux with a_{spike}. (bottom) Predicted flux (equation (3.18)) versus simulated flux. Experimentally determined coefficients are $k = 0.8$ kg s^2 m^{-4}, $K_a = 0.07$kg s m^{-2} and $a_{crit} \approx 1$ m s^{-2}.

Parameters c_f, $\tan f$ and e_b are of particular interest. Choice of c_f is problematic; we adopt $c_f = 0.003$, following *Thornton et al.* [1996] and *Gallagher et al.* [1998], but note that the range of c_f is 0.001 to 0.006 [*Church and Thornton*, 1993; see also *Faria et al.*, 1998]. Spherical simulation particles have an experimentally determined angle of repose of 25º, which corresponds to $\tan f = 0.47$, a slight departure from conventional usage of $\tan f = 0.63$ [*Bagnold*, 1956] for natural grains. Using these values and our simulation results in (3.19), we find the bedload efficiency $e_b = 1.03$, substantially greater than $e_b = 0.12$ suggested by *Bagnold* [1966] for 1.1-mm-diameter grains in unidirectional flows having a velocity of ~1 m s^{-1}. *Gallagher et al.* [1998] found that model skill for offshore bar migration at Duck was maximized for $e_b = 0.135$ for sediment having a mean diameter of 0.13 mm and that model skill was relatively insensitive to e_b.

3.5. Conclusions

Transient pressure gradients generated by the passage of surface gravity waves in the surf zone produce episodes of intense sheet flow bedload transport. Existing energetics-based models can be modified to account for these pressure gradient effects by including a single acceleration term that is readily calculated from fluid motion measurements obtained in field studies. The bedload efficiency derived from simulations is nearly an order of magnitude greater than that suggested by *Bagnold* [1966].

Chapter 4

Discrete Particle Model for Sheet Flow: The Effects of Gentle Slopes on Bedload Transport in the Surf Zone

4.1. Introduction

The general problem is the lack of reliable and robust sediment transport equations for use in models for evolution of nearshore morphology. The primary objective of this study is to quantify the effects of small arbitrary local slopes on bedload transport under unsteady flow conditions typical of the surf zone. A discrete particle model [*Drake and Calantoni*, 2001] is used to simulate bedload transport over beds arbitrarily oriented with respect to the flow direction for unsteady unidirectional flows. Considering the dynamics of saltating grains due to shear stress from a steady flow (as in a river channel), *Sekine and Parker* [1992] showed that for slopes transverse to the flow direction the bedload flux down the transverse slope is directly proportional to the sediment flux along the flow direction. Similarly, simulations of intense sheetflow transport under unsteady flow conditions typical of the surf zone also show the bedload flux down the transverse slope is directly proportional to the sediment flux along the flow direction for transverse slopes. This general approach to the problem of bedload transport along transverse sloping beds gives the reader the ability to implement the transport formula of choice along the flow direction while still offering a

prediction of transport down the local transverse slope. One example of the failure of current models for use in the surf zone [e.g. – *Bailard and Inman*, 1981] is illustrated in the following case; for a purely cross-shore flow, the Bailard model predicts only transport along the direction of flow. Our simulations demonstrate what might be intuitively obvious, that is, purely cross-shore flow will induce alongshore transport down a slope that is perpendicular to the flow direction. Despite the triviality of this conclusion, there still are no models for use in the surf zone that address this issue.

The bedload transport formulae presented here will be important to anyone who wants to model the morphology of bed forms in the surf zone (like bar migration, megaripples, rip channels, and even smaller scale features). Given the mechanism presented in this paper, strong alongshore currents measured in the vicinity of the bar crest [*Feddersen et al.*, 1998; *Ruessink et al.*, 2001] would effect bar migration rates while promoting a broad and smooth bar during times of no bar motion. Prediction of the rate of bar migration, for example, may be improved by considering the additional cross-shore bedload transport that may result from a strong alongshore current parallel to the bar crest. The future goal is to use the results of our deterministic grain-scale discrete particle model to drive a larger scale statistical model of surf zone evolution.

4.1.1. Bedload Transport Models

Several bedload transport formulae have been developed to predict transport under unsteady flow conditions typical of the surf zone [*Bowen*, 1980; *Bailard and Inman*, 1981; *Ribberink*, 1998; among many others]. While several of these formulae treat descriptors of fluid motion as vector quantities, all incorporate the effects of gravity only in one direction. *Kovacs and Parker* [1994] offered a vectorial bedload transport formula for use in river

channels that treats the gravitational force as an arbitrary vector; indeed, cross-channel slopes in rivers are often one or more orders of magnitude greater than the water surface slopes generating downstream flow. The question needs to be raised as to whether the effect of gravity on bedload transport rates differs from steady flows to unsteady flows. Clearly, the literature is lacking information about the effects of sloping beds on bedload transport under unsteady flow conditions.

Energetics models of *Bowen* [1980] and *Bailard* [1981] are vectorial in their presentation; however, in practice they are only used for prediction of cross-shore profile evolution in the surf zone [*Thornton et al.*, 1996; *Gallagher et al.*, 1998]. As the discussion pertains to bedload transport in the surf zone, some of the deficiencies of these models have been detailed along with offering a modification term for the Bailard formulation in *Drake and Calantoni* [2001]. The previous study is limited to bedload transport over horizontal beds. *Bailard's* model [1981] allows for the input of a single value for the bed slope, $\tan b$, where b represents the angle of the cross-shore profile. While it allows for waves to propagate at varied angles to the shoreline it does not allow the user to define an arbitrary local bed slope. This study will restrict itself to two limiting cases: the first case will outline a general formula for incorporation of a slope, a, that is perpendicular to the flow direction, while the second limiting case will restrict the local slope, b, to be along the flow direction (Figure 4.1). The physical framework for the development of a vectorial bedload transport formula will be outlined.

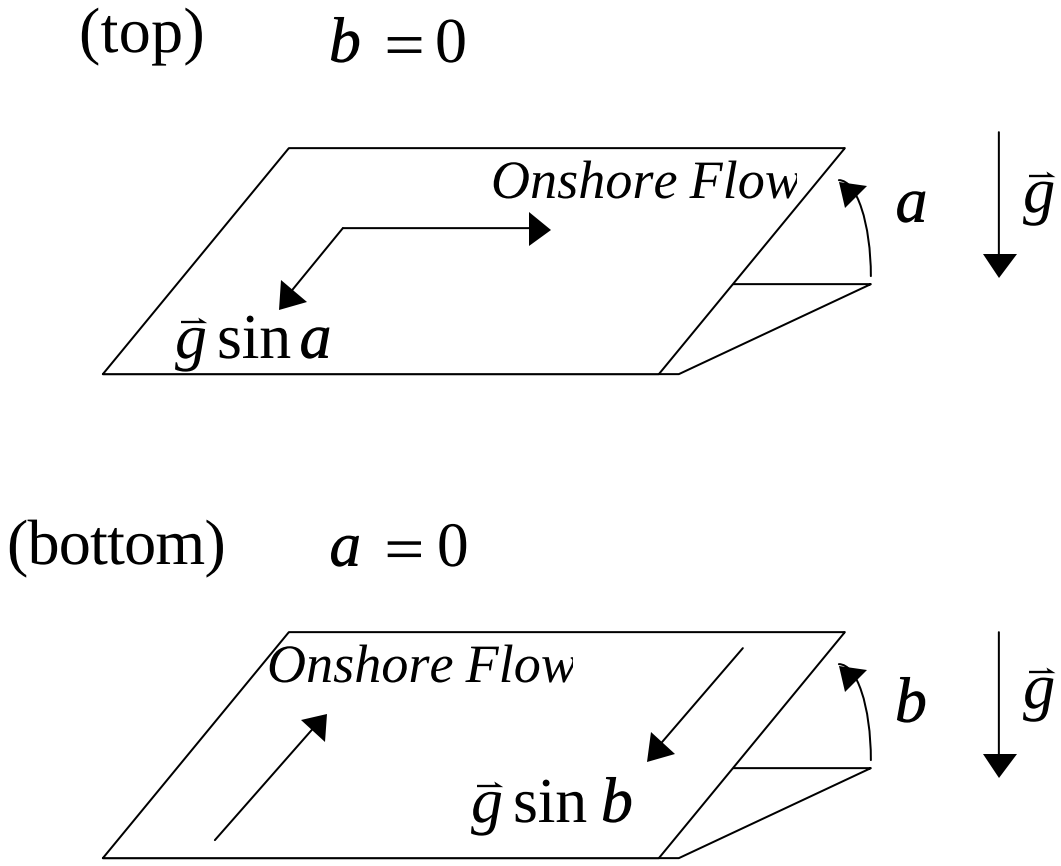

Figure 4.1. (top) The flow is perpendicular to the local slope in this case. The transverse flux will always be down the local slope regardless of the sign of a. (bottom) In this second limiting case the slope is along the flow direction. The slope, b, can take positive and negative values. In simulations a negative value of b represents a wave propagating shoreward and downhill.

4.2. Discrete Particle Model

A discrete particle model used to simulate bedload transport under a range of unsteady flow conditions typical of the surf zone is detailed in *Drake and Calantoni* [2001]. Here we will offer a brief description of the mechanics of the model while taking more time to discuss some of the key assumptions and limitations of the model's applicability to the field.

Sediment particles in the model are represented as discrete spheres that may move in all three dimensions. Essentially, normal and tangential forces between contacting spheres are modeled with springs and sliding friction, respectively. The fluid is modeled in one dimension as a stack of thin slabs. The fluid slabs exchange momentum via an eddy viscosity determined from a mixing length model. Pressure gradient forces generated by the progression of an idealized surface gravity wave drive fluid and particle motion. The fluid and particles are coupled via fluid-particle forces of buoyancy, drag, and virtual mass [for more details see *Drake and Calantoni*, 2001].

4.2.1. Model Assumptions

The flow modeled here is strictly oscillatory, back and forth along a single direction. There is no steady current super-imposed on the oscillatory flow. The physical domain of the model encloses a finite volume in the boundary layer and assumes that the hydrodynamic conditions be constant across this simulation domain (~2 cm in length). Simulations utilize periodic boundaries in the two horizontal directions with a rigid bottom in the vertical direction, located well below the level of moving particles. Flow considered parallels to the nominally planar at rest bed surface, which can be oriented arbitrarily up to the angle of

repose. An appropriate coordinate system and pair of angles necessary to specify an arbitrarily oriented bed is defined in section 4.4.5.1.

The model limits itself solely to the simulation of bedload transport as sheet flow and assumes that grain-grain interactions dominate the physics of the granular flow at these high sediment concentrations > 8% [*Bagnold*, 1954]. There is a size distribution with a 1.1-mm mean diameter that is similar to that of *King* [1991]. Simulations previously run with this grain size distribution over both horizontal and gently sloping beds show favorable agreement with the experiments of *King* [1991] and are shown in Figure 4.2.

4.3. Simulation of Surf Zone Conditions Over Sloping Beds

A suite of simulations is performed to explore the two limiting cases of bed angle $a = 0$ with b varying and vice versa (see Figure 4.1). The waveforms simulated are from the same suite simulated over a horizontal bed in *Drake and Calantoni* [2001]. The pressure gradient force in all cases is proportional to a truncated Fourier series,

$$F(t) \propto \sum_{i=0}^{4} \frac{1}{2^i} \sin\left[(i+1)wt + if\right], \tag{4.1}$$

where f is the waveform parameter corresponding to the biphase [e.g., *Elgar and Guza*, 1986; *Elgar and Chandran*, 1993] and w is the angular frequency, $w = 2p/T$. All waveforms simulated over sloping beds have a period, T = 6 s. The maximum fluid velocity amplitude is varied from 0.5 to 1.5 m s^{-1}, while the waveform parameter f is varied from 0 to $p/2$, grossly representing the range of skewed to asymmetric waves, respectively. Figure 4.3 shows how the time series of the near bed fluid velocity evolves as f changes from 0 to $p/2$,

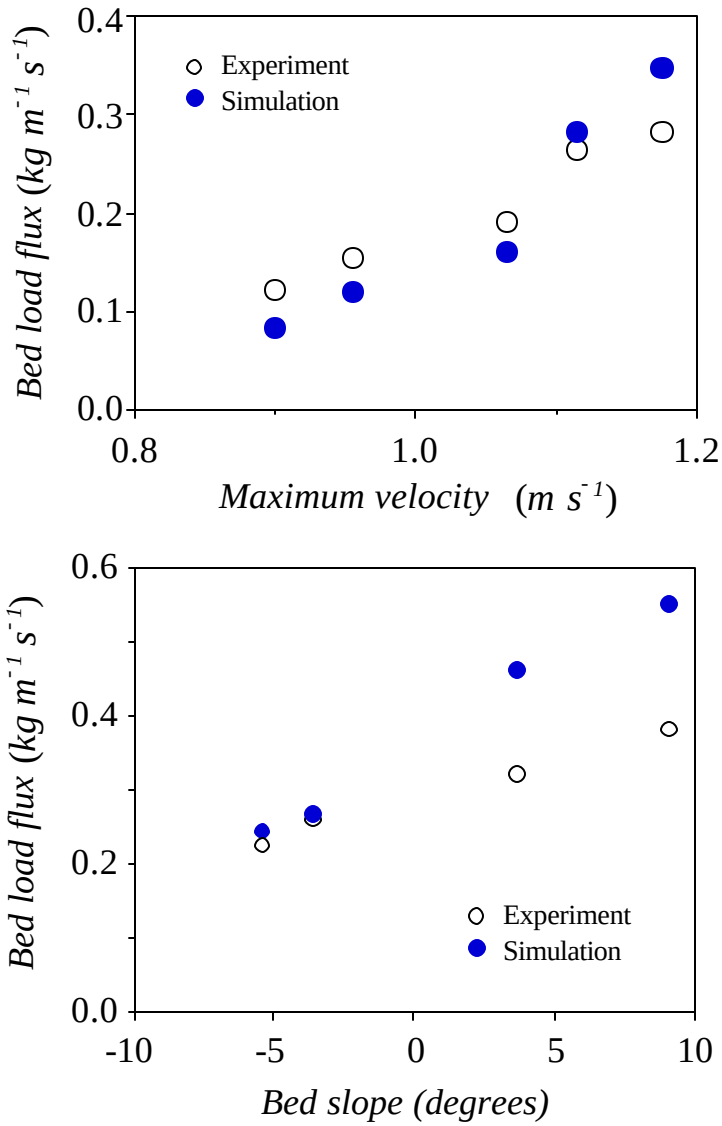

Figure 4.2. (top) Shows comparison with *King's* [1991] data taken in an oscillatory flow tunnel for a horizontal bed. Half-period sine waves with a period of about 5 seconds are shown with natural sand having a grain size distribution with a median of 1.1mm. (bottom) Shows comparison with *King's* [1991] data over a sloping bed for the maximum free stream velocity of 1.1 m s^{-1} with the same period and grain size as the top. In all cases shown the simulated flux values are always within a factor of 2 of those measured experimentally.

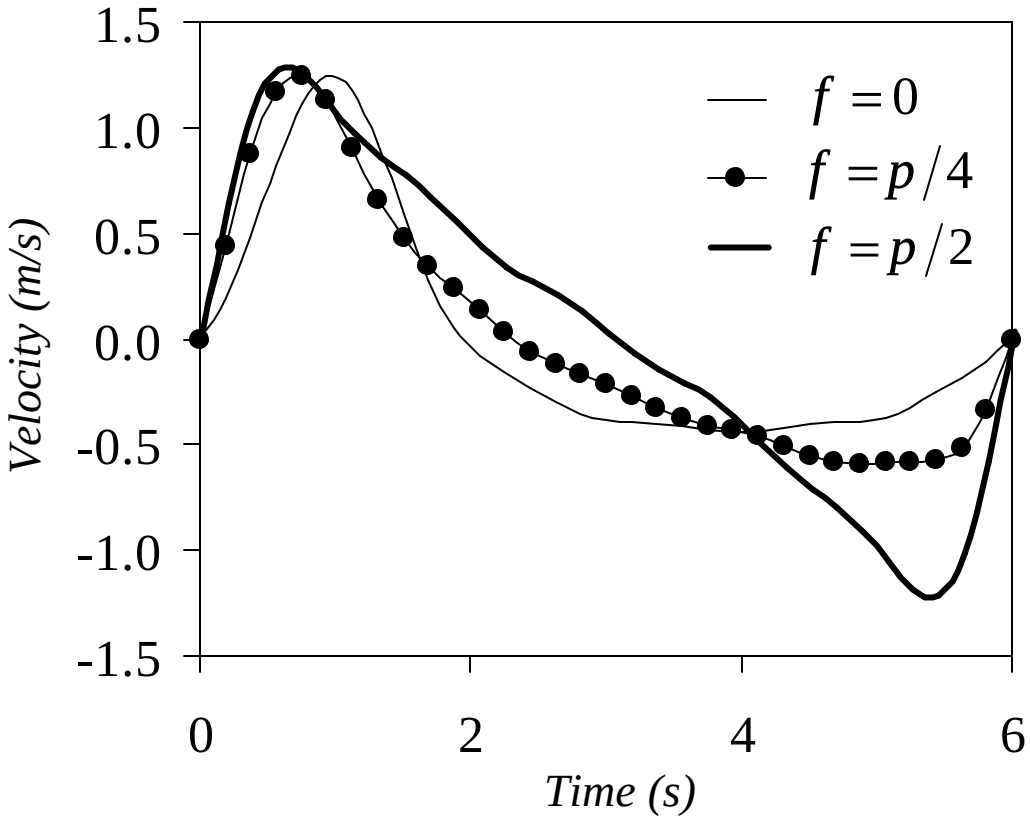

Figure 4.3. As the waveform parameter, f, is varied from 0 to $p/2$ the shape of the velocity time series near the bed goes from skewed to asymmetric, grossly representing the range of conditions from shoaling to broken waves with the $f = p/2$ waveform representing the sawtooth characteristic of surf zone bores.

grossly representing the range of surf zone conditions from a shoaling wave to a bore.

4.3.1. Beds Sloping Transverse to the Flow Direction

Simulations explore two limiting cases of beds sloping both along and transverse to the flow direction. First consider the case of $b = 0$, which corresponds to maintaining a horizontal bed along the direction of wave propagation (top Figure 4.1), while gradually increasing the transverse slope, a. While the simulations correctly describe the physics of particle interactions at angles up to and exceeding the angle of repose, these high angles are not common in the surf zone, except, perhaps on bed form slip faces. We have limited ourselves to the simulation of small angles in this study, up to 10°.

4.3.1.1. Simulation Results

The results of simulations with $b = 0$ and a varying are shown in Figure 4.4. The range of conditions represented here includes monochromatic waves with maximum velocity amplitudes from 1.0 m s^{-1} up to 1.5 m s^{-1}, velocity skewness [*Elgar et al*., 1988] ranging from 0 to 1.2, and a period of 6 seconds. The transverse bed slope, a, is given in radians and is plotted against the ratio of transverse flux to net flux along the flow direction in Figure 4.4 (top). In Figure 4.4, a Δ represents waveforms that yield episodes of bedload flux under both the onshore and offshore directed portion of the wave, while waveforms represented by a • only have an onshore episode of bedload flux. The ratio of transverse flux to the net flux along the flow direction appears to increase linearly with increasing transverse bed slope for both the Δ and •, with the rate of increase being greater for the waves represented by the Δ. When the ratio of transverse flux to total flux along the flow direction (sum of the magnitudes of onshore and offshore flux) is plotted (bottom Figure 4.4) instead of the net

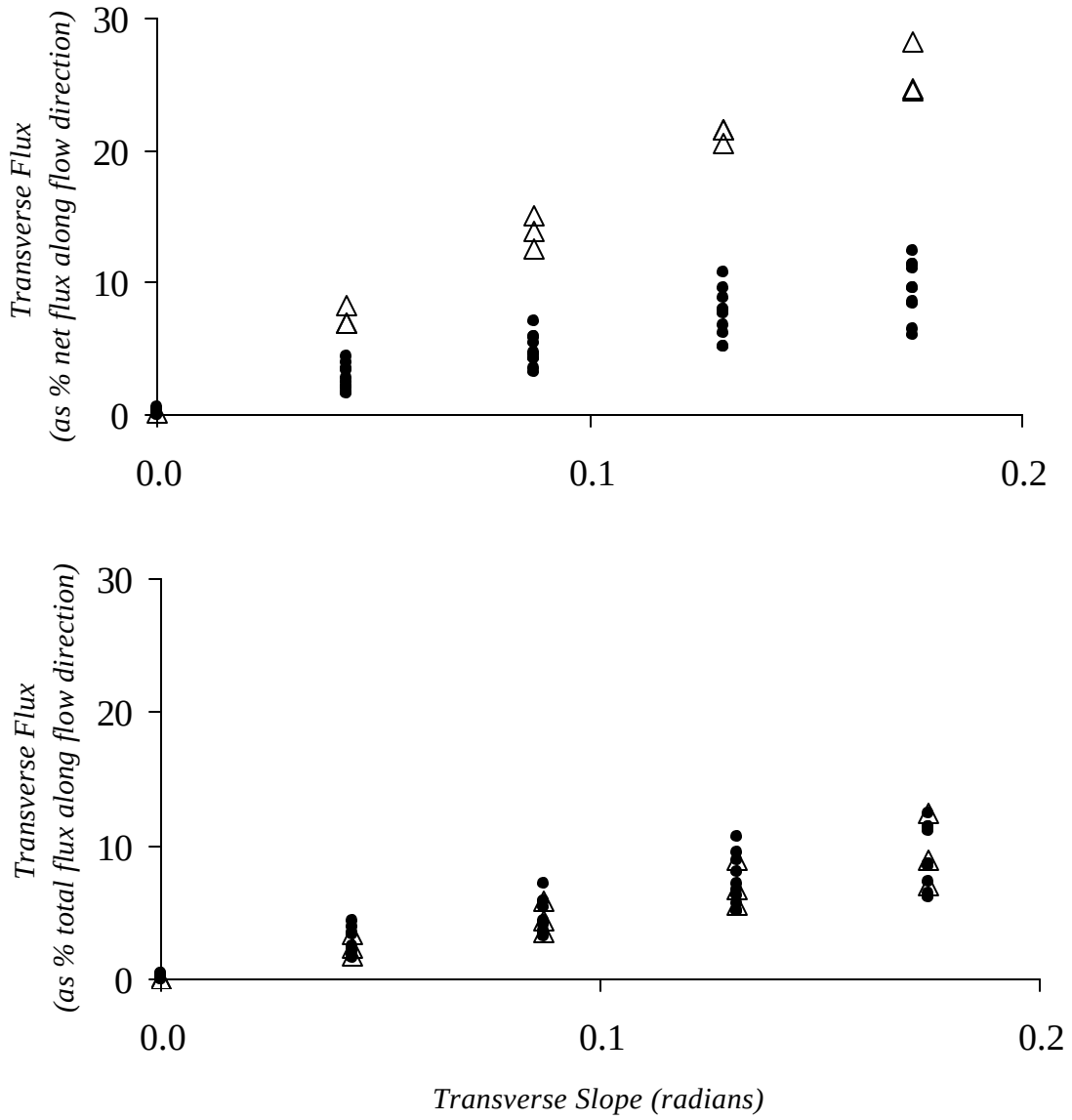

Figure 4.4. Monochromatic waves with 6 s periods, maximum velocity amplitudes ranging from 0.5 to 1.5 m s^{-1} and velocity skewness values from 0 to 1.2 are shown. The slope along the flow direction, $b = 0$, while the transverse bed slope, a (given in radians), is varied discretely from 0 to 10°. The bedload flux down the transverse slope is plotted as a percentage of the net flux (top) and total flux (bottom) measured along the flow direction. Waves with velocity skewness = 0 are represented by Δ, while all other waveforms are represented by •. Only waves with velocity skewness at or near zero, Δ, exhibit episodes of both onshore and offshore bedload flux.

flux along the flow direction for all waveforms simulated, the rate of increase of the flux ratio with increasing transverse bed slope can be represented by a single value (linear regression performed below). For waveforms represented by a Δ, since grains move down the transverse slope during each half of the wave period, one needs to use the total flux along the flow direction to predict the transverse flux. In simulations discussed below, as you grow the period of waves (represented by a Δ) from 6s out to 12s, the net flux tends to zero along the flow direction, necessitating the need to predict flux on a half period basis. The effects of varying the wave period while holding all other parameters constant will be discussed later in section 4.4.

In order to predict transverse flux due to a local slope perpendicular to the flow direction, one must predict flux along the flow direction on a half wave period basis and use the magnitude of the total flux. A simple linear regression of the Figure 4.4 (bottom) shows the magnitude of the transverse flux can be quantified as a function of flux along the flow direction with the relationship,

$$q_t = k a q_c, \tag{4.2}$$

where q_t is the transverse flux, q_c is the sum of the magnitudes of flux along the flow direction during a single wave period, a is the alongshore slope in radians, and $k = 0.5$ is a numeric constant.

4.3.2. Beds Sloping Along the Flow Direction

The second limiting case explored with the simulations has a horizontal bed in the transverse direction ($a = 0$) and varies the slope, b, along the direction of fluid flow (bottom Figure 4.1). This case breaks down further into waves propagating up and down the local

slope, represented by positive and negative values of b, respectively. The symmetry of the problem in the transverse direction is apparent, however, it is not so along the flow direction. In simulations the reduction in transport due to wave propagation up a local slope is not usually equal and opposite the increase in transport due to wave propagation down a local slope of the same magnitude. This asymmetry in transport rates along the flow direction manifests itself through the skewness of the near bed velocity field. As the skewness of a monochromatic wave changes from 0 to a maximum value (~1.2 in this study) the dependence of the net transport rate on the slope deviates from linearity. The differences in observed transport rates in the simulations are shown and the physical mechanisms responsible are discussed and quantified in the following sections.

4.3.2.1. Simulation Results

The second limiting case has the alongshore angle, $a = 0$, with b varying from -10º to 10º where the positive b values represent waves propagating up the beach face. Monochromatic waves with a 6 second period having no steady current superimposed are simulated with the form of the pressure gradient given in (4.1) where the maximum fluid velocity amplitude takes values of 0.75, 1.0, and 1.25 m s^{-1}, while the velocity skewness takes the values of 0, 0.4, 0.8, 1.1, and 1.2. For the maximum velocity amplitude of 1.25 m s^{-1} all values of the velocity skewness are plotted for the range of slopes in Figure 4.5. The sawtooth waveform (velocity skewness = 0) is the only wave with maximum velocity amplitude of 1.25 m s^{-1} that yields episodes of both onshore and offshore flux over a horizontal bed. Two different mechanisms responsible for the onshore and offshore-directed flux are identified and discussed below. In spite of this complex behavior, the sawtooth

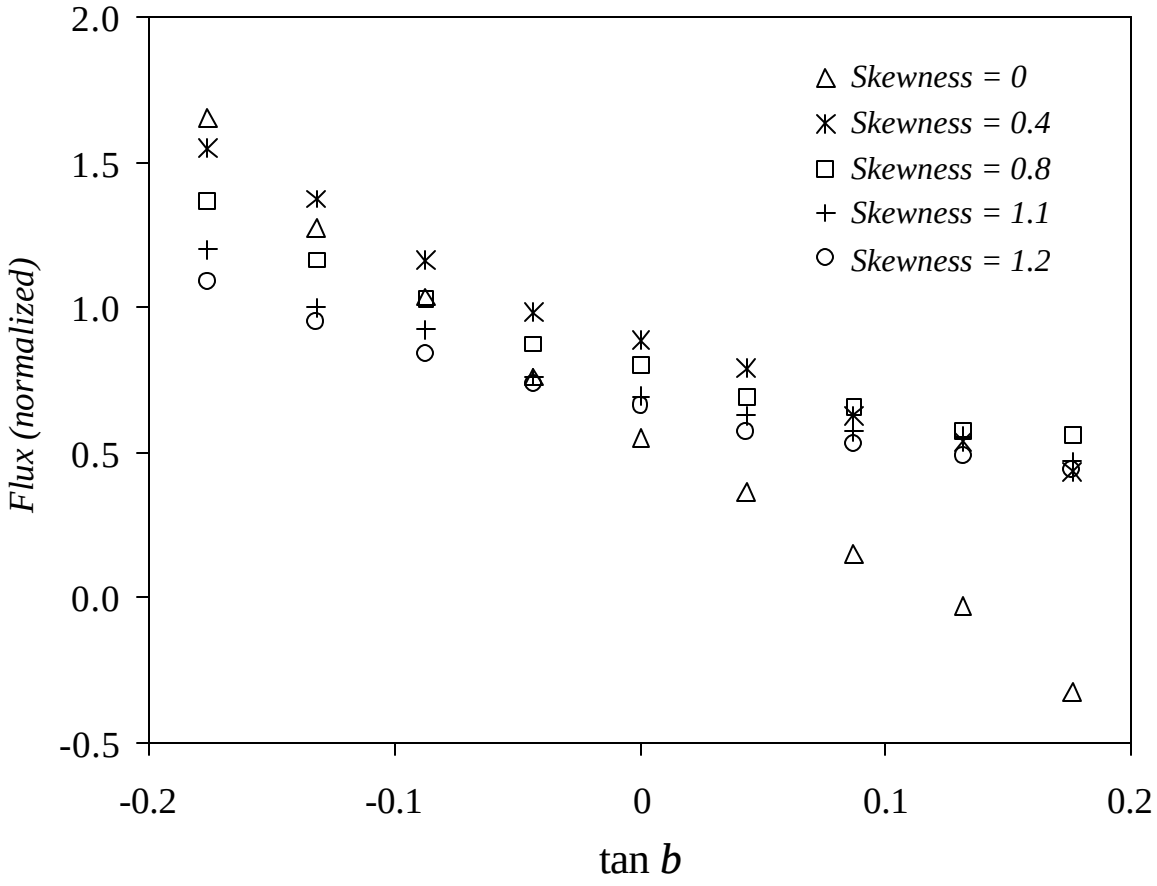

Figure 4.5. Plotted above is the net bedload flux (normalized by a constant) versus the tangent of the bed slope, b, along the flow direction. For all simulation data points shown the wave period is 6 seconds, the maximum velocity amplitude is 1.25 m s^{-1}, and the transverse bed slope, $a = 0$. The sawtooth waveform (velocity skewness = 0) shows a linear dependence of the net flux on the local bed slope, while all the other simulated waveforms appear to deviate from this linearity as the bed slope is increased from –10º to 10º.

waveform is the only wave simulated that exhibits a linear dependence of net flux (time averaged over one complete wave period) on local slope across the entire range shown. As soon as the velocity skewness becomes nonzero the dependence of the net flux on the local slope deviates from linearity with increasingly positive slope. This behavior poses difficulty in finding a suitable parameterization that captures the appropriate functional dependence exhibited by the model. The results are presented and discussed here with no parameterization offered.

The time series of bedload flux measured in simulations shows that the sawtooth waveform exhibits both an onshore and offshore episode of flux (top Figure 4.6). We previously have proposed that strong horizontal pressure gradients due to the passage of surface gravity waves act as impulsive forces on the boundary layer and serve as the physical mechanism responsible for the episode of onshore flux. In the parameterization of our data we did not discuss the mechanism responsible for the observed offshore episodes of flux. It was reasonable to ignore these offshore episodes of flux over a horizontal bed since they did not exceed about 20% of the onshore flux for the range of conditions simulated [*Drake and Calantoni,* 2001].

4.3.2.2. Offshore Flux Under Asymmetric Waves

During the offshore portion of the wave, the near bed fluid acceleration is nearly constant and much smaller in magnitude than the onshore spike, which has the effect of slowly increasing the offshore fluid velocity (top Figure 4.6). Under these conditions the physical mechanism dominating observed offshore episodes of bedload flux in simulations is the particle drag force. Inspection of the offshore portion of the flux time series over a horizontal bed for the sawtooth waveform shows that incipient motion doesn't occur until

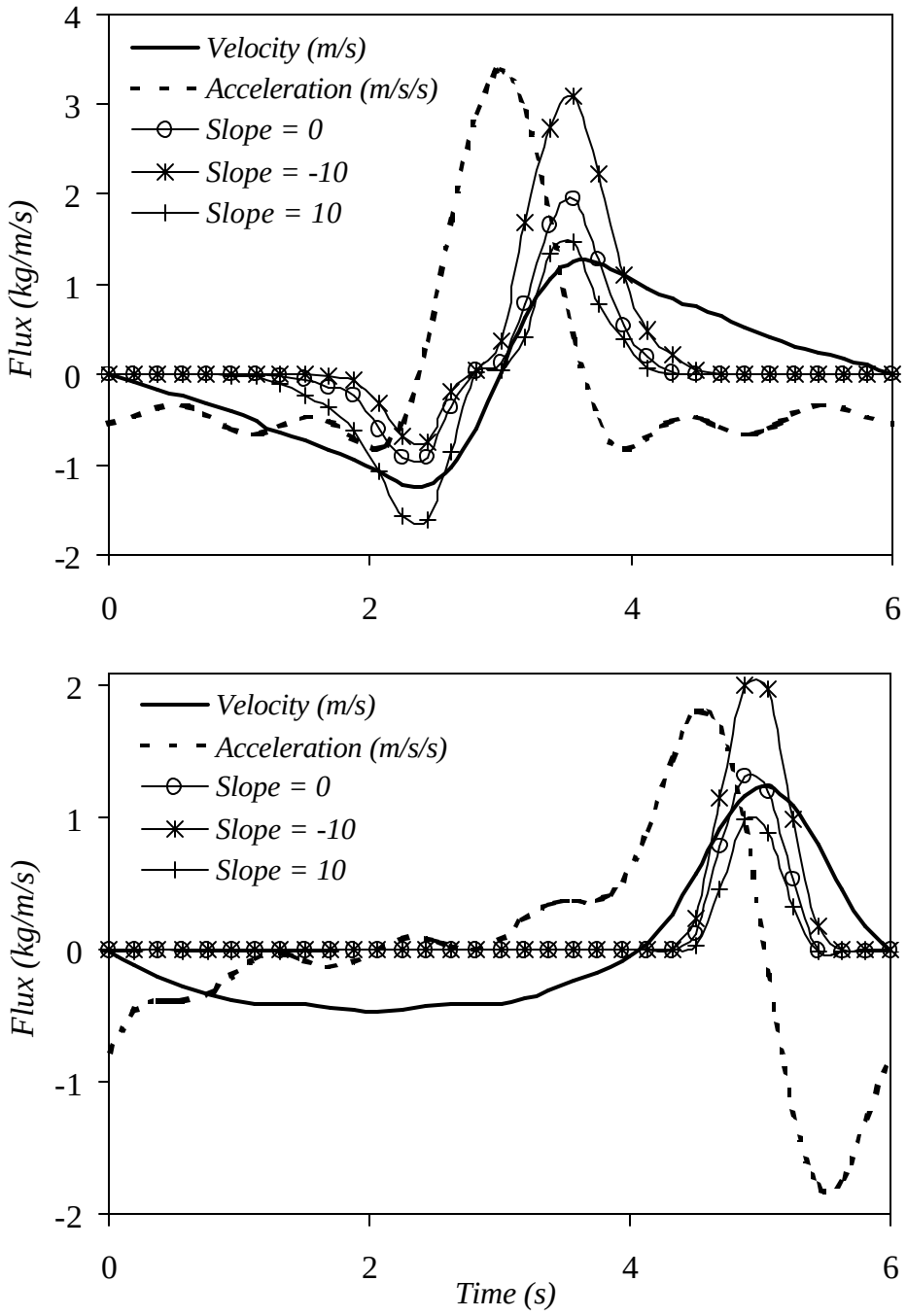

Figure 4.6. (top) Time series for the sawtooth waveform (velocity skewness = 0) and (bottom) the skewed waveform (velocity skewness = 1.2) of the fluid velocity and bedload flux. Here the alongshore angle, a=0, while the cross-shore angle, b, is varied from –10° to 10°. The wave period is 6 seconds and shown is the second complete wave period from the simulation.

the magnitude of the instantaneous velocity exceeds about 0.8 m s^{-1} (top Figure 4.6). A simple criterion chooses the point of incipient motion at the time when the instantaneous flux value exceeds 0.1 kg m^{-1} s^{-1}, roughly corresponding to a bedload layer thickness of 1 to 2 grains diameters in the simulations. The critical Shields parameter for incipient motion may be written as,

$$q_c = \frac{t_c}{(r_s - r)gD} = \frac{c_f u_c^{\,2}}{(s-1)gD}, \tag{4.3}$$

where t_c is the critical shear stress, s is the relative density ($s = r_s / r$), g is gravity, D is the nominal grain diameter, c_f is the drag coefficient, and u_c is the critical free stream velocity. For the simulation over a horizontal bed in Figure 4.6 (top) the known parameters have the values of $s = 2.65$, g = 9.8 m s^{-1}, D = 0.0011 mm, and $u_c \approx$ 0.8 m s^{-1}. A value of 0.05 for the critical Shields parameter on a horizontal planar bed would require the value of the drag coefficient, $c_f = 0.0015$, which lies within the range of commonly accepted values for use in the field [*Church and Thornton*, 1993; *Faria et al.*, 1998].

The sawtooth waveform with maximum velocity amplitude of 1.25 m s^{-1} has an offshore velocity maximum greater than the about 0.8 m s^{-1} needed to induce sheet flow over a horizontal bed in simulations. Studying just the offshore portion of the wave shows the presence of the slope directly affects the critical value of the fluid velocity for incipient motion. *Fredsoe and Deigaard* [1992] calculated the effect of a local slope on the critical Shields parameter under a particle drag dominated transport regime for the two limiting cases examined in this study. In simulations, during the offshore portion of the sawtooth waveform, the presence of a +/- 10º slope will result in approximately a 20% reduction/increase in the

critical free stream velocity from the critical value for incipient motion over a horizontal bed which is consistent with the predictions of *Fredsoe and Deigaard* [1992] (see section 4.4.5.1).

4.3.2.3. The Slope Effect on Impulse Induced Transport

The previously proposed physical mechanism for onshore transport under monochromatic waves is the horizontal pressure gradient. The initiation and duration of the onshore flux episode is relatively unaffected by the presence of the local slope for the range of slopes simulated, while the peak flux value exhibits a nonlinear dependence on the slope (see Figure 4.6). The peak onshore flux increases by approximately 50% from the value over a horizontal bed for a slope of -10° while only experiencing about a 25% decrease from the value over a horizontal bed for the slope of 10° for both of the limiting values of velocity skewness simulated. The effect of the local slope along the flow direction on the flux is not symmetric for impulses propagating up and down slopes of the same magnitude. A qualitative discussion of this observation is given below.

4.4. Discussion

The results from the discrete particle model presented here show the utility in this type of approach to the problem of bedload transport. Without doing any physical experiments, insight into how to quantify the mechanisms responsible for bedload transport has been gained and some parameterization of simulated transport rates has been accomplished.

4.4.1. Slopes Transverse to Flow Direction

The relationship presented in equation (4.2) will be immediately useful for models of surf zone morphology. It gives the modeler the flexibility of choosing any bedload transport formula for predicting flux along the flow direction while still offering a consistent prediction of the flux induced by the transverse slope. While this result is an empirical observation from the simulation data and has not been rigorously derived, *Sekine and Parker* [1992] have presented a mathematical relationship derived from a saltating bedload transport model for transverse sloping beds under steady flow conditions analogous to equation (4.2). Qualitatively, this result may seem like an obvious conclusion since the only force acting to transport sediment down the lateral slope is gravity, which for small bed slopes is just proportional to the slope. Likewise, the only material available for transport is that which is mobilized due to the flow and flux along the flow direction.

4.4.2. Slopes Along Flow Direction

Bedload transport over beds sloping along the flow direction can be described with two independent physical mechanisms for each of the onshore and offshore-directed episodes of flux. *Madsen* [1974] showed the horizontal pressure gradient under the passage of a steep wave front induces failure of the bed for conditions typical of the surf zone. On the backside of these steep front waves is a low amplitude, offshore directed, acceleration that has the effect of slowly increasing the offshore velocity. The particle drag force is the primary mechanism for bedload transport during this portion of the wave. Strong horizontal pressure gradients acting on the boundary layer are the primary mechanism for the impulse-induced episode of onshore bedload flux [*Drake and Calantoni*, 2001]. It has been shown that the presence of a local slope along the flow direction affects the resulting bedload transport due

to each mechanism differently. The difficultly then arises in finding a suitable parameterization for the net transport rate that incorporates the different physical mechanisms and how they are affected by the presence of a local slope.

4.4.3. Dependence of the Net Transport Rate on Wave Period

Presenting a suitable parameterization for the slope effects described in this paper is compounded by the effect of a varied wave period. Simulations were performed over horizontal beds that hold all wave parameters constant, while changing the wave period from 6 seconds to 12 and 3 seconds. At this time, none of these longer and shorter period waves have been simulated over sloping beds. The net transport rates for the horizontal bed can still be reasonably predicted by a modified Bailard formulation [*Drake and Calantoni*, 2001] for the range of periods simulated (Figure 4.7). The foreseeable problems lie in the observed offshore episodes of bedload transport that occur under waves with large maximum velocity amplitude and small velocity skewness. This drag dominated regime of bedload transport becomes much more important for the longer period waves. For the sawtooth waveform with a 12 second period and maximum velocity amplitude of 1.5 m s^{-1}, the net transport rate over a complete period approaches zero on a horizontal bed. Having shown above that a small local slope along the flow direction will effect the magnitude of the onshore and offshore flux in different ways, one sees that the traditionally linear dependence on local slope will be wholly inadequate for this type of waveform common to the surf zone.

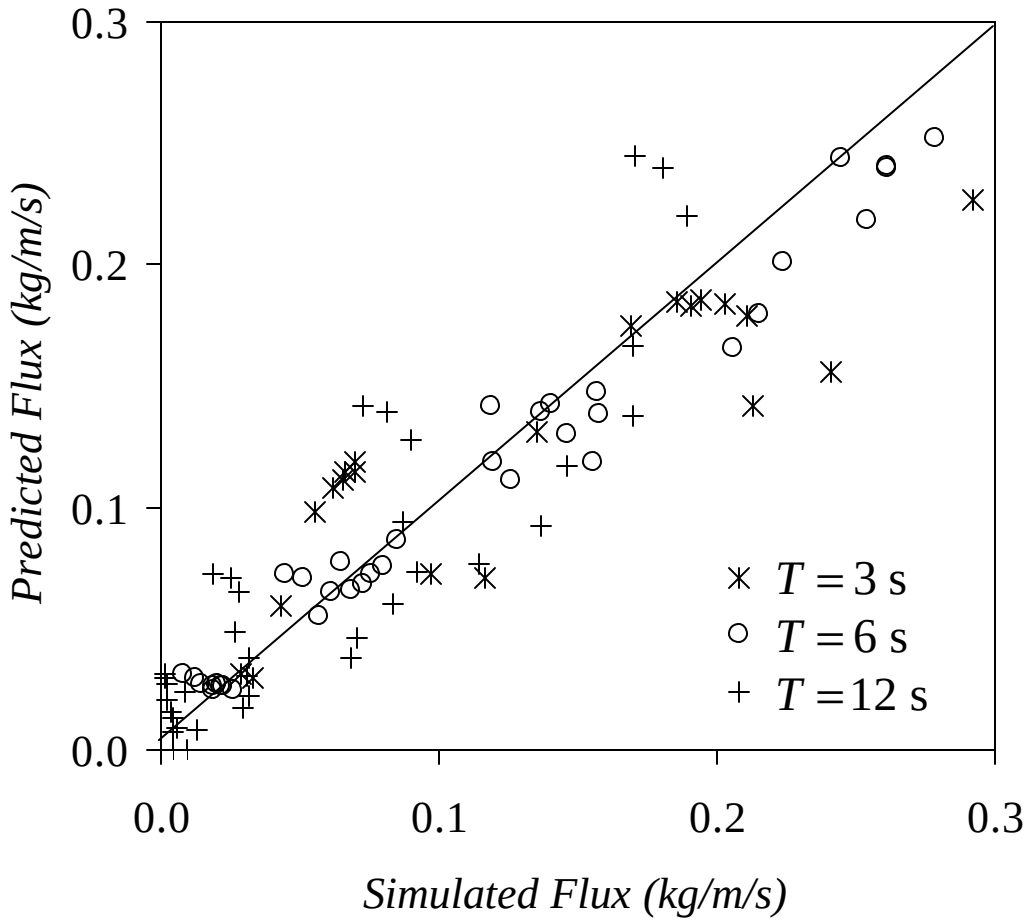

Figure 4.7. The parameterization of bedload flux previously proposed for 6 s period waves under a range of unsteady flow conditions does appear to offer some reasonable predictions of the net flux when tested against simulation results for waves of 3 s and 12 s periods with all other wave parameters (and grain size) being held constant.

4.4.4. Effects of Particle Shape on Bedload Transport

In the discrete particle model sediment grains are modeled as spheres with the material properties of quartz. Modeling sediment particles as spheres offers many advantages computationally to any non-spherical alternative. The most notable physical property that is measurably different in the spherical approximation of a sand grain is the angle at which the internal friction is overcome, which is referred to here as the angle of repose, Φ. For a typical bed of spheres in the simulations the angle of repose is $\Phi \approx 26°$. This is determined by slowly rotating the force of gravity from a position normal to the bed (representing a horizontal bed) into a plane perpendicular to the resting bed. Natural sand grains have been shown to have an angle of repose of $\Phi \approx 32°$ [*Bagnold*, 1956]. We note this difference in the angle of repose so that the local bed angles simulated can be taken in the proper context when being compared directly to natural sand at the same angle. Physical experiments [*Drake et al*., 1991] have shown that the bulk properties of a collision-dominated bedload layer are largely independent of particle shape. We acknowledge that simulations with spherical particles may poorly predict the initiation and cessation of motion; however, for sheet flow generated by large waves, the model gives favorable prediction of bulk transport rates (see Figure 4.2).

4.4.5. A New Formulation for Bedload Transport

Here we will discuss the framework for a new formulation to predict bedload transport under unsteady flow conditions over sloping beds. There are two physical mechanisms outlined in this paper responsible for the observed episodes of onshore and offshore flux. It seems reasonable that a complete bedload transport formula would have two parts; one term for the impulsive onshore flux episode and another term for the particle drag

dominated offshore flux episode. The sum of the two terms will provide an appropriate net transport rate. Each of the two terms would have a decidedly different dependence on the wave period and the local slope along the flow direction. The simulations presented in this chapter show a nonlinear dependence between the peak flux and the bed slope along the flow direction for the impulsive onshore flux episode, while the slope effects on the initiation of motion in the particle drag regime appear to be already quantified by the existing literature. During the offshore episodes of flux the wave period dependence at a given maximum velocity amplitude becomes much more pronounced. The critical Shields parameter is exceeded for a much longer time during the offshore directed portion of a 1.0 m s^{-1} sawtooth wave with a 12 second period than one with a 6 second period. Likewise, the onshore spike in fluid acceleration, previously used to quantify the onshore flux episode, is decreased as the period grows with all other wave parameters held constant.

4.4.5.1. Dependence of Critical Shields Parameter on Local Slope

Determining the effect of an arbitrary local slope on the critical Shields parameter is an essential component for the development of a vectorial bedload transport formula. *Fredsoe and Deigaard* [1992] derived two separate formulas for the critical Shields parameter for the two limiting slope cases simulated in this study (Figure 4.1). The relationships are derived considering a transport regime dominated by the particle drag force. Simulations show offshore episodes of bedload flux under unsteady flow conditions are dominated by the particle drag force. Predicting flux under these conditions over an arbitrarily sloping bed necessitates a relationship that explicitly includes the two angles needed to specify the orientation of the local bed to the local direction of gravity.

Definition of the Bed Angles.

The Euler matrix, $\vec{\mathrm{A}}$, for rotations [p. 147, *Goldstein,* 1980] reduces to

$$\vec{\mathrm{A}} = \begin{pmatrix} \cos b & \sin b & 0 \\ -\cos a \sin b & \cos a \cos b & \sin a \\ \sin a \sin b & -\sin a \cos b & \cos a \end{pmatrix}, \tag{4.4}$$

with Ψ=0, Φ replaced with b, and Θ replaced with a. Choose your space coordinates right-handed with the gravity vector, $\vec{g}$, along the negative y-axis. Align the positive x-axis such that the unit vector, $\hat{u}$, pointing in the direction of wave propagation (onshore for waves simulated here), lies in the xy-plane. The angle between the positive x-axis and the vector, $\hat{u}$, is given by b and can take positive or negative values. This corresponds to the first rotation and now $\hat{u}$ points along the positive x′-axis. The angle a specifies the second rotation of the local plane, which is about the x′-axis. The value of $\vec{g}'$, the components of $\vec{g}$ in the reference frame of the bed, can be obtained by

$$\vec{g}' = \vec{\mathrm{A}} \begin{pmatrix} 0 \\ -\mathrm{g} \\ 0 \end{pmatrix} = -\mathrm{g} \begin{pmatrix} \sin b \\ \cos a \cos b \\ -\sin a \cos b \end{pmatrix}. \tag{4.5}$$

Calculation of the Critical Shields Parameter.

In the coordinate system defined above the magnitude of the maximum stabilizing force of the bed is given by,

$$\left|\vec{F}_S\right| = W m_s \cos a \cos b \ , \tag{4.6}$$

where W is the immersed weight and $m_s = \tan\Phi$ is the friction coefficient for a sediment particle on the bed. If one considers only the particle drag force as a mobilizing force, then at

the initiation of motion the magnitude of the sum of the drag force and the gravitational force must equal the magnitude of the maximum stabilizing force (equation (4.6)),

$$\left|\vec{F}_D + \vec{F}_G\right| = \left|\vec{F}_S\right|. \tag{4.7}$$

Substitution into equation (4.7) yields,

$$W m_s \cos a \cos b = \sqrt{(-F_D - W \sin b)^2 + W^2 \sin^2 a \cos^2 b}\ , \tag{4.8}$$

considering that the quasi-steady flow occurs during the offshore portion of the wave and for positive values of b this flow is down slope and along the negative x′-axis. Expansion of equation (4.8) and rearranging terms gives the following,

$$\frac{F_D{}^2}{W^2 m^2{}_s} + \frac{2F_D \sin b}{W m^2{}_s} + \frac{\sin^2 b + \sin^2 a \cos^2 b}{m^2{}_s} - \cos^2 a \cos^2 b = 0. \tag{4.9}$$

Using the definitions of F_D and W given by *Fredsoe and Deigaard* [1992] leads to the expression,

$$\frac{q^2{}_c}{q^2{}_{co}} + \left(2\frac{\sin b}{\tan \Phi}\right)\frac{q_c}{q_{co}} + \frac{\sin^2 b + \sin^2 a \cos^2 b}{\tan^2 \Phi} - \cos^2 a \cos^2 b = 0, \tag{4.10}$$

where q_{co} and q_c are the critical Shields parameter over a horizontal and sloped bed, respectively. This equation (4.10) may be solved with the quadratic formula and choosing the positive solution results in the following expression for the critical Shields parameter,

$$q_c = q_{co} \cos b \left(\cos a \sqrt{1 - \frac{\tan^2 a}{\tan^2 \Phi}} - \frac{\tan b}{\tan \Phi}\right). \tag{4.11}$$

Consider the first limiting case investigated (top Figure 4.1) with b = 0. The expression for the critical Shields parameter (4.11) reduces to

$$q_c = q_{co} \cos a \sqrt{1 - \frac{\tan^2 a}{\tan^2 \Phi}}\ , \tag{4.12}$$

which is consistent with example 7.3 in *Fredsoe and Deigaard* [1992]. Here the effect will be to always lower the value of the critical Shields parameter from its value over a horizontal bed regardless of the sign of a. The maximum simulated alongshore angle, $a = 10°$, gives a value of $q_c = 0.91 q_{co}$. Considering the expression for q_c given by equation (4.3) along with a similar expression for q_{co} allows for the dependence of the critical free stream velocity on the local slope to be directly calculated. The case of $b = 0$ and $a = 10°$ gives less than a 5% decrease in the critical free stream velocity for that over a horizontal bed. Likewise, in simulations the time averaged flux along the flow direction is not measurably effected by slopes in the alongshore direction.

Consider the second limiting case investigated (bottom Figure 4.1) with $a = 0$. In this case, the expression for the critical Shields parameter (4.11) reduces to

$$q_c = q_{co} \cos b \left(1 - \frac{\tan b}{\tan \Phi}\right), \tag{4.13}$$

which is consistent with example 7.4 in *Fredsoe and Deigaard* [1992]. Here the effect of the slope changes with the sign of b, that is, the critical Shields parameter is increased when the particle drag force opposes the component of gravity along the bed and decreased when the particle drag force acts in the same direction as the component of gravity along the bed. For simulation conditions ($\Phi \approx 26°$), substituting a value of $b = 10°$ ($b = -10°$) gives approximately a 22% reduction (16% increase) in the critical free stream velocity for that over a horizontal bed during the offshore directed portion of the wave. This is roughly consistent with the simulation results shown in Figure 4.6 (top); the offshore critical free

stream velocity, u_c, over a horizontal bed has an observed value of $u_c \approx 0.80$ m s^{-1}, while this value is reduced to $u_c \approx 0.64$ m s^{-1} for $\beta = 10°$ and increased to $u_c \approx 0.96$ m s^{-1} for $\beta = -10°$.

Application of Result.

No new physics has been derived in equation (4.11); rather, two separate expressions previously provided by *Fredsoe and Deigaard* [1992] have been combined into one general formula for the coordinate described above. This general expression for the critical Shields parameter will be a necessary component for the development of a vectorial bedload transport formula that allows for an arbitrarily sloping bed to the flow direction. The simulation results presented in this paper show that even under highly unsteady flow conditions there will exist episodes of bedload transport that can be modeled accurately considering just the particle drag force. The real challenge lies in identifying these episodes on a wave-by-wave basis and finding a suitable parameterization that captures the relevant physics.

4.5. Conclusions

The desire to develop morphologic models of coastal evolution necessitate improved formulae for the prediction of sediment transport over arbitrarily sloping beds under combined wave and current flows for a complete range of sediment sizes (from fine to cobbles). This study has focused on the bedload transport of coarse sediment over gently sloping beds both along and transverse to an unsteady flow with no superimposed current. A complete vectorial bedload transport equation is not offered, but a relationship that predicts bedload flux down slopes transverse to the flow direction in terms of the flux along the flow direction is given. The mechanisms responsible for bedload flux under unsteady fluid motion

are described and have been previously parameterized over horizontal beds. The framework for the development of a new bedload transport formula has been outlined and will serve as a blueprint for future work.

Chapter 5

Discrete Particle Model: Approximating the Shape of Natural Particles

5.1. Introduction

The "strength of the bed" is a difficult concept to define and quantify. Qualitatively, the strength of the bed represents the ability of a granular assemblage to resist motion under a stress applied along a direction tangential to the surface. *Bagnold* [1956] proposed that the ratio of the tangential shear stress to normal dispersive stress is equal to the friction coefficient for a bed of granular material. The static value given by *Bagnold* [1956] for natural sand is $m = \tan\Phi = 0.63$, which gives a critical angle, $\Phi \approx 32°$. Here the critical angle is that at which a pile of natural sediment grains will experience failure solely under the influence of gravity. For a static pile of grains, the critical angle may be used to quantify of the strength of the bed. Previously, in the discrete particle model natural sand grains are being modeled as individual spheres. The results are encouraging and the spherical approximation to the shape of a natural sand grain does allow for bedload transport rates to be reasonably predicted under intense sheet flow conditions. However, predictions of the initiation and cessation of motion may be hindered. The critical angle for a bed of identical spheres in the simulations is found to have a value, $\Phi \approx 26°$. A clear discrepancy exists

between the critical angle of natural sediment and the value exhibited by the discrete particle model with spherical elements. The hypothesis is that the strongest influence on "bed strength" is particle geometry or shape. I will test this hypothesis by modeling the shape of natural sand grains with "composite particles" (described in section 5.2 below) constructed from pairs of overlapping spheres. The motivation for choosing to construct non-spherical particles in this manner is largely guided by the fact that for the composite particle the moments of inertia are solvable analytically in the appropriate coordinate system. Additionally, the existing code that detects contacts between individual spheres can be utilized.

5.2. The Composite Particle

A non-spherical particle with one axis of symmetry, a composite particle, is constructed by allowing two spheres of radius R_1 and R_2 to overlap, where $R_1 \geq R_2$. The intersection of the surfaces of the two spheres defines a circle lying in a plane perpendicular to the line joining the centers of the two spheres. The origin of the body coordinate system for the composite particle is first chosen at the center of this circle of intersection. The inertia tensor is calculated and the parallel axis theorem is used to find the principle moments about the center of mass (CM) of the composite particle.

5.2.1. Volume Calculation

A cylindrical coordinate system with the positive z-axis pointing from the center of sphere 1 to the center of sphere 2 is a suitable choice of body coordinates for performing the volume integration of the composite particle (see Figure 5.1). The plane $z = 0$ separates the composite particle into two partial spheres allowing the volume integration to be separated

into a sum over the two partial spheres, $V = V_1 + V_2$. Using the cylindrical body coordinate system for the composite particle defined in Figure 5.1 this volume integral becomes

$$V = \int_0^{\sqrt{R_1^2-(z+R_1\cos g_1)^2}} r dr \int_0^{2p} dq \int_{-R_1(1+\cos g_1)}^{0} dz \; + \int_0^{\sqrt{R_2^2-(z+R_2\cos g_2)^2}} r dr \int_0^{2p} dq \int_0^{R_2(1-\cos g_2)} dz \,. \quad (5.1)$$

Performing the integration yields,

$$V = \frac{p}{3}\left[R_1^3\left(2+3\cos g_1 - \cos^3 g_1\right) + R_2^3\left(2-3\cos g_2 + \cos^3 g_2\right)\right], \quad (5.2)$$

the volume of the composite particle.

5.2.2. The Principle Moments of Inertia

The inertia tensor for the composite particle can now be found using the body coordinate system with the integration limits on the volume defined above. The inertia tensor in any coordinate system can be represented by the following equation from *Goldstein* [equation (5.8), 1980],

$$I_{jk} = \int_V r(\vec{r})(r^2 d_{jk} - x_j x_k) dV \,. \quad (5.3)$$

The density, $r(\vec{r})$, will be considered constant over each partial sphere. In cylindrical coordinates $x_1 = r\cos q$, $x_2 = r\sin q$, $x_3 = z$, $dV = r dr dq\, dz$, and $r = \sqrt{x_1^2 + x_2^2}$. Each integral in equation (5.3) must be performed as a sum of volume integrals using the same form and limits found in equation (5.1). Performing the integrations gives a diagonal inertia tensor of the form,

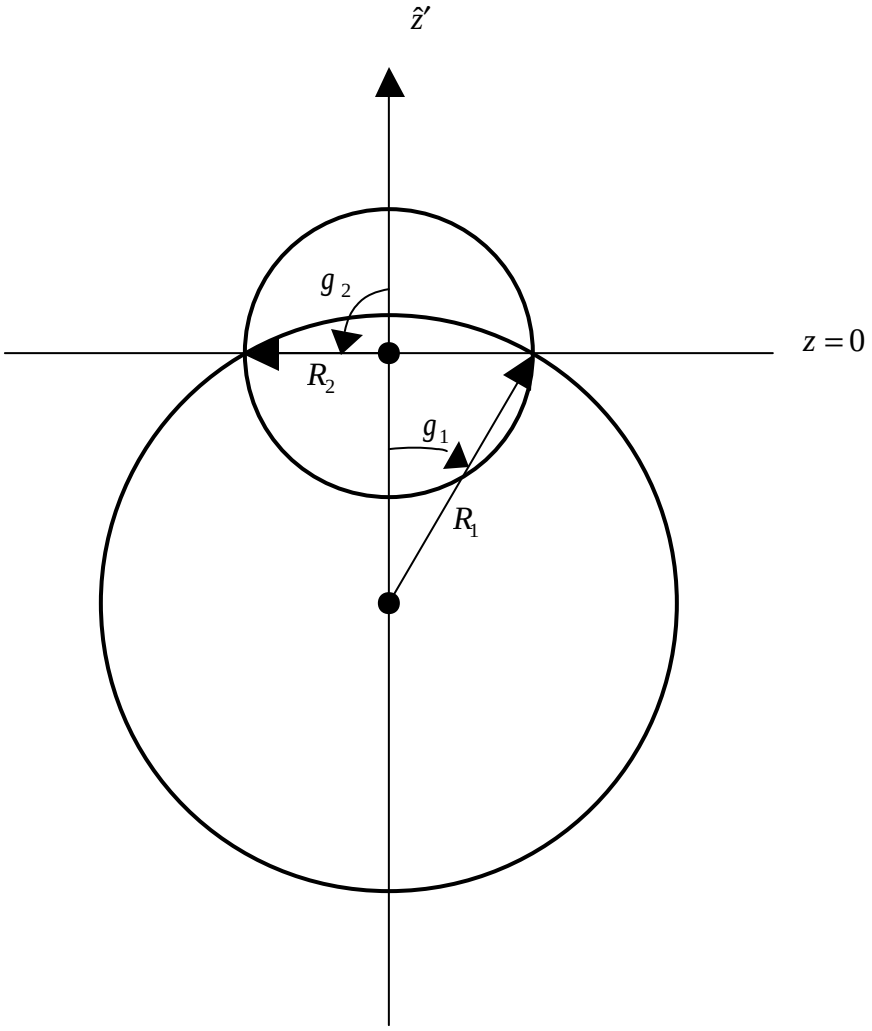

Figure 5.1. Shown is a composite particle in plan view (maximum projected area). The origin for the coordinate system is chosen at the center of the circle of intersection of the two partial spheres. The two partial spheres are separated by the plane $z = 0$. The angles γ_1 and γ_2 are measured down from the positive *z*-axis about the center of each respective partial sphere. The inertia tensor is solved about the origin shown above by doing the volume integrations in cylindrical coordinates. The parallel axis theorem is then used to find the moments of inertia about the CM of the composite particle.

$$\vec{\vec{I}} = \begin{pmatrix} I_1 & 0 & 0 \\ 0 & I_2 & 0 \\ 0 & 0 & I_3 \end{pmatrix}, \tag{5.4}$$

where

$$I_1 = \frac{\rho r_1 R_1^5}{60}\left[(1+\cos\gamma_1)\left(16+29\cos\gamma_1+11\cos^2\gamma_1-\cos^3\gamma_1+\cos^4\gamma_1\right)\right]$$

$$+\ \frac{\rho r_2 R_2^5}{60}\left[(1-\cos\gamma_2)\left(16-29\cos\gamma_2+11\cos^2\gamma_2+\cos^3\gamma_2+\cos^4\gamma_2\right)\right], \tag{5.5a}$$

$$I_2 = I_1, \tag{5.5b}$$

and

$$I_3 = \frac{\rho r_1 R_1^5}{30}\left[(1+\cos\gamma_1)\left(8+7\cos\gamma_1-7\cos^2\gamma_1-3\cos^3\gamma_1+3\cos^4\gamma_1\right)\right]$$

$$+\ \frac{\rho r_2 R_2^5}{30}\left[(1-\cos\gamma_2)\left(8-7\cos\gamma_2-7\cos^2\gamma_2+3\cos^3\gamma_2+3\cos^4\gamma_2\right)\right]. \tag{5.5c}$$

5.2.3. The *z*-coordinate of the CM

The choice of the body coordinate system in Figure 5.1, along with the condition that each partial sphere has uniform density, guarantees that the position of the CM will be along the *z*-axis. The position of the CM for the composite particle is found by first integrating to obtain the *z*-coordinate of the CM of each partial sphere. Following example 8.1 found in *Marion and Thornton* [1988] the position of the CM of partial sphere 1 and 2 are given by the following integrals,

$$z_1' = \frac{r_1 \rho}{M_1}\int_{-R_1(1-\cos\gamma_1)}^{0} z\left(R_1^2-\left(z+R_1\cos\gamma_1\right)^2\right)dz, \tag{5.6a}$$

$$z_2' = \frac{r_2 p}{M_2} \int_0^{R_2(1-\cos g_2)} z\left(R_2^2 - \left(z + R_2 \cos g_2\right)^2\right) dz\,, \tag{5.6b}$$

where M_1 and M_2 are the masses of partial sphere 1 and 2, respectively. Performing the integration gives the following values of the z-coordinate of the CM for each partial sphere,

$$z_1' = -\frac{r_1 p\, R_1^4}{M_1}\left(\frac{1}{4} + \frac{2}{3}\cos g_1 + \frac{1}{2}\cos^2 g_1 - \frac{1}{12}\cos^4 g_1\right), \tag{5.7a}$$

$$z_2' = \frac{r_2 p\, R_2^4}{M_2}\left(\frac{1}{4} - \frac{2}{3}\cos g_2 + \frac{1}{2}\cos^2 g_2 - \frac{1}{12}\cos^4 g_2\right). \tag{5.7b}$$

Now the z-coordinate of the CM for the composite particle is given by

$$z_{cm}' = \frac{1}{M_1 + M_2}\left(M_1 z_1' + M_2 z_2'\right). \tag{5.8}$$

5.2.4. The Principle Moments of Inertia About the CM

The inertia tensor found in equation (5.4) is given about the origin of the body coordinate system described in Figure 5.1. In general, the CM of the composite particle does not coincide with this choice of origin and the parallel axis theorem is used to find the principle moments of inertia about the CM. Applying the parallel axis theorem, the principle moments of inertia about the CM of the composite particle shown in Figure 5.1 become

$$I_1' = I_1 - (M_1 + M_2)\, z_{cm}^2 \tag{5.9a}$$

$$I_2' = I_2 - (M_1 + M_2)\, z_{cm}^2 \tag{5.9b}$$

$$I_3' = I_3\,. \tag{5.9c}$$

5.3. Modifications to Code

The discrete particle model used in *Drake and Calantoni* [2001] has been modified to simulate the composite particle described above. Natural sand grains, previously modeled as spherical elements, are now modeled with composite particles. At present there is no existing user manual for the code. Future work will include the development of a detailed description of the code. Below is a brief description of how the existing framework was modified to compute composite particles.

5.3.1. Contact Detection and Forces

For the purposes of detecting contacts between composite particles and the forces generated at those contact points, the code views each composite particle as two individual spheres. This allows for all the existing machinery performing these tasks to be utilized. For a chosen sphere, when the code loops over all particles in the simulation to determine its nearest neighbors, the loop excludes its composite companion. This insures that the two spheres comprising the composite particle do not interact with each other. The forces generated at the contact points for each individual sphere are given in terms of a normal spring force and a tangential friction force. These contact forces are then re-expressed in terms of the normal and tangential components relative to the CM of the respective composite particle. For each individual force determined to be tangential to the CM of a composite particle, a moment arm is constructed and the torque is calculated. The sum of the torque on each composite particle is then calculated along with the sum of the force through the CM. The force through the CM is passed on to the predictor/corrector time stepping

routine and $\vec{F} = m\vec{a}$ is used to calculate the resulting translational motion of the composite particle. Computing the resulting rotational motion is slightly more complicated.

5.3.2. Rotational Motion of the Composite Particle

In the simulation, the position and orientation of each composite particle are tracked relative to a fixed origin, the space coordinate system for all particles. The resulting rotation of a composite particle will occur about its CM and is determined by solving Euler's equations of motion for a rigid body. However, the net torque about the CM of a composite particle has been found relative to the space coordinate system. Therefore, the components of the torque in the body coordinate system for each composite particle must be found before Euler's equations can be solved. The components of the net torque in the body coordinate system of the composite particle are found by performing a coordinate transformation using the body axis unit vector, $\hat{z}'$, tracked in the fixed space coordinate system. The resulting changes in the rotational velocity are found in the body coordinate system for each composite particle and then rotated back to the space coordinate system before being time stepped. The new orientation of the composite particle is updated by performing the resulting rotation on the body axis unit vector, $\hat{z}'$.

5.4. Quantifying the Shape of Natural Particles

Scientists have constructed many different "shape factors" with the assumption that the shape of a natural particle can be closely approximated by a triaxial ellipsoid. The majority of work performed to date towards classifying the shape of natural particles has been largely motivated by the desire to find a functional relationship between shape and the settling velocity [*Dietrich*, 1982]. The motivation in this study is to construct a composite

particle (described above) that exhibits the same critical angle (or internal angle of friction) as natural beach sand. Here the shape of composite particles will be quantified by the sphericity as defined by *Wadell* [1932]. For the composite particles in simulations the value of sphericity is calculated exactly as the ratio of the diameter of a sphere with the equivalent volume to the diameter of the circumscribed sphere. Although the Wadell sphericity is a preferred parameter for the purposes of this study, it does not accurately represent the settling behavior of natural particles and therefore is not as widely used as the Corey Shape Factor or the Maximum Projection Sphericity for sediment shape classification [*Middleton and Southard*, 1984, *Blatt et al.*, 1972]. Natural particles will assume a value between 0 and 1 for all the shape factors mentioned above. The physical limits of the composite particle range from a sphere to a dumbbell shown in Figure 5.2. For this range of shapes the Wadell sphericity assumes values from 0.63 to 1, the Corey Shape Factor assumes values from 0.71 to 1, and the Maximum Projection Sphericity assumes values from 0.79 to 1.

5.5. Simulations with Composite Particles

A suite of simulations is performed for a group of composite particles that span the possible range of sphericity values. The critical angle is measured for 8 different beds of 250 identical composite particles, formed by fixing the value of the ratio of R_2:R_1 and then allowing the value of g_2 (defined in Figure 5.1) to vary from 0 to π in $\pi/8$ increments (see Figure 5.3.) A value of R_1=2.5 mm is chosen with the value of the ratio R_2:R_1=0.5. All simulations here are performed for particles under the influence of gravity in a vacuum; there is no interstitial fluid being modeled. Simulations begin by settling the particles from a

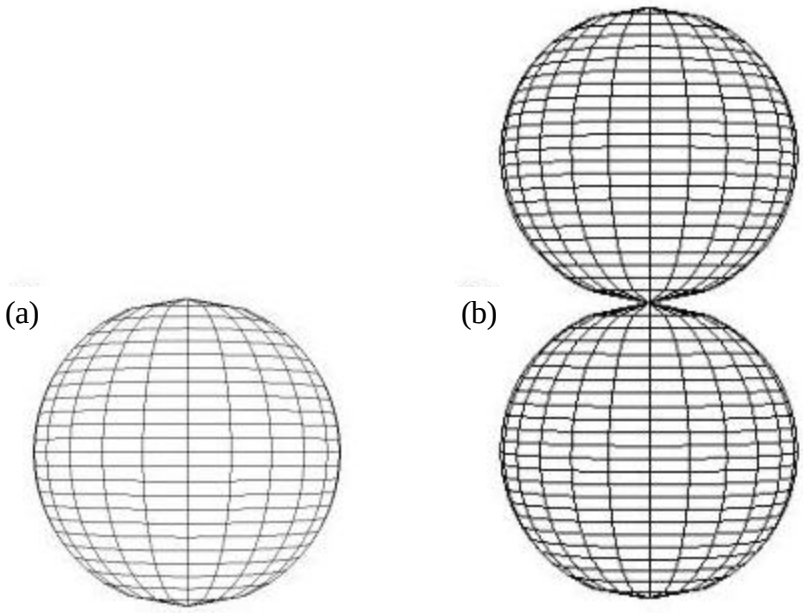

Figure 5.2. The physical limits of the composite particle range from the (a) sphere to the (b) perfect dumbbell. The perfect dumbbell ($R_2=R_1$, $g_2 = p$) represents the lowest possible value of sphericity, $S = 0.63$, allowed for a composite particle. The perfect dumbbell is distinguished from a dumbbell ($R_2<R_1$, $g_2 = p$) shown in Figure 5.3(d).

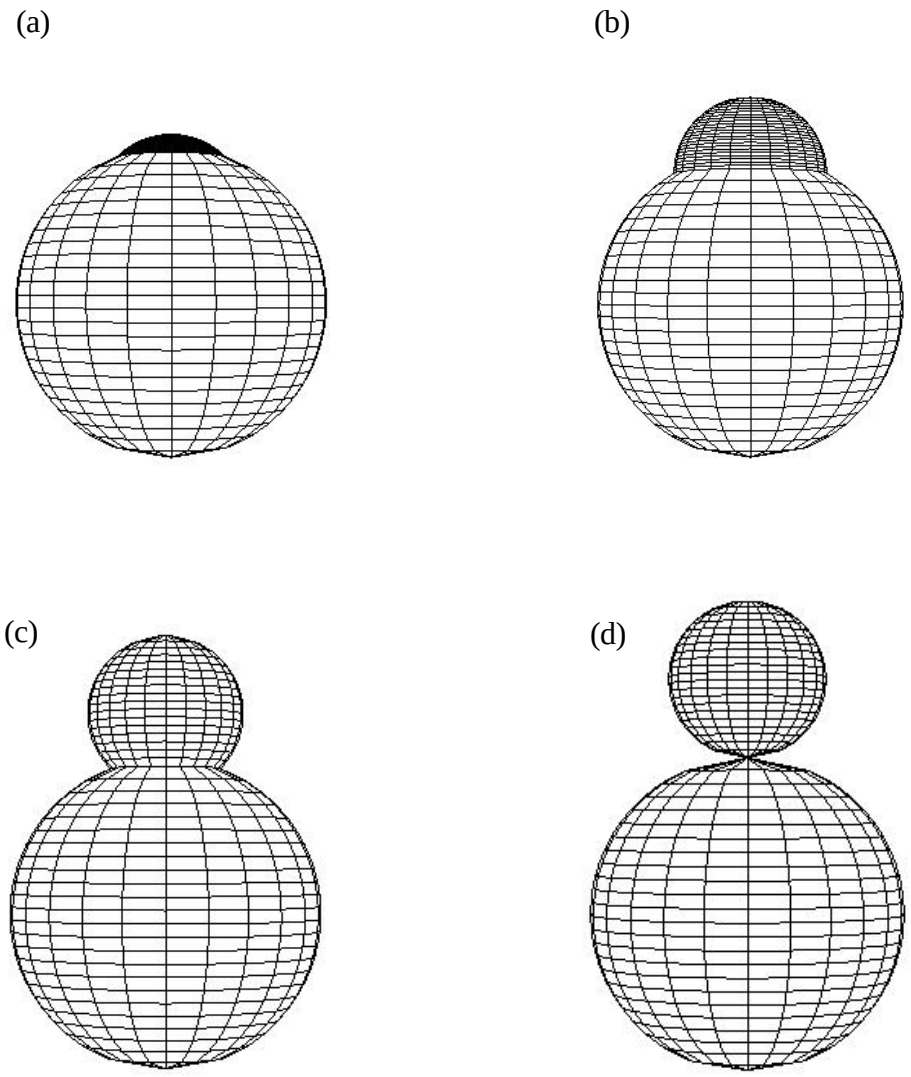

Figure 5.3. The ratio, R_2:R_1=0.5, is constant for all the particles shown here. For $g_2 = 0$ the composite particle becomes a sphere (not shown). For the particles shown (a) $g_2 = p/4$, $S = 0.96$, (b) $g_2 = p/2$, $S = 0.86$, (c) $g_2 = 3p/4$, $S = 0.74$, (d) $g_2 = p$, $S = 0.69$, where S is the sphericity. Also simulated but not shown for the same ratio are composite particles with $g_2 = p/8, 3p/8, 5p/8, 7p/8$.

regular lattice onto a smooth basal plane having a row of spherical stoppers attached to prevent the wholesale sliding of the granular assemblage. Periodic boundary conditions are used in the two lateral dimensions. Tilting the bed until failure is accomplished by rotating the gravity force vector from a position normal to the bed along the direction normal to the row of fixed stoppers until failure. Once failure is achieved, the gravity vector is rotated back similarly until it is again orthogonal to the bed. The gravity vector is rotated in discrete time intervals; every second the angle of inclination of the bed is increased by 0.1º. It was found that one second of real time is sufficient for complete failure of the bed to develop, allowing for the critical angle to be measured with a precision of 0.1°.

5.5.1. Simulation Results

The simulations performed demonstrate that there exists some range of composite particle shapes that do exhibit the same critical angle as natural beach sand. The critical angle is plotted as a function of the sphericity in Figure 5.4. Each point is the average value of 10 consecutive simulations with one standard deviation plotted above and below. A bed of identical composite particles with the ratio, R_2:R_1=0.5, $g_2 = 5p/8$, having sphericity, $S = 0.8$, exhibit an average critical angle of 32.9°. By varying the ratio, R_2:R_1, and value of g_2 other composite particles with similar sphericity value may be constructed. Some preliminary simulations demonstrate that other composite particles with sphericity, $S \approx 0.8$, also exhibit a critical angle similar to natural sand, showing some promise that sphericity may serve as an adequate shape parameter for quantifying the critical angle of a bed of composite particles.

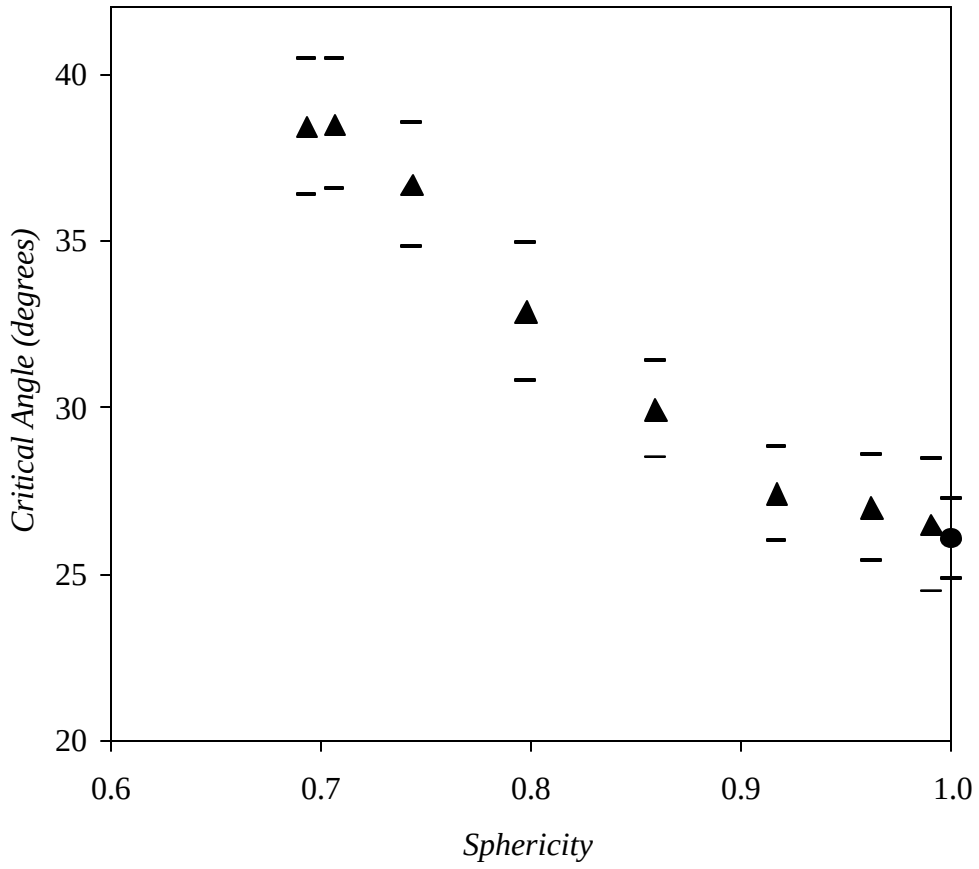

Figure 5.4. Each ▲ is the average critical angle of 10 successive simulations with one standard deviation plotted above and below each point for the ratio, R_2:R_1=0.5, with the value of g_2 increasing smoothly from $p/8$ to p with decreasing sphericity. The ● represents the critical angle for a bed of identical spheres. Note that the composite particle with the ratio, R_2:R_1=0.5, $g_2 = 5p/8$, and sphericity, $S = 0.8$, exhibits an average critical angle of 32.9° almost identical to natural beach sand.

5.5.1.1. Critical Angle for Spheres

Simulations to measure the critical angle of a bed of identical spheres are performed in exactly the same manner as the composite particles. The value of the critical angle for a bed of 250 identical spheres with radius, R=2.5 mm, is found to be 26° (shown in Figure 5.4.) While this value is greater than the proposed theoretical value of 23.5° [*Albert et al.*, 1997; *Barabasi et al.*, 1999], it is in exact agreement with experiments performed with glass beads inside rotating drums. *Jaeger et al*. [1989] found the average critical angle of glass beads to be 26°, independent of container or grain size.

5.6. Discussion of Application to Bedload Transport Modeling

Non-spherical particles are constructed from pairs of overlapping spheres. It is shown that a bed of identical, so-called, composite particles, may exhibit the same critical angle as natural beach sand. The next step in this study is to use composite particles in simulations of bedload transport in the surf zone. While the model presented here appears to adequately calculate all particle-particle interactions, the fluid-particle interactions for composite particles with the existing slab model [*Drake and Calantoni*, 2001] need to be specified before one-to-one comparisons can be made between bedload transport rates of simulations with spheres and composite particles.

5.6.1. Drag Force

The modeling of the drag force exerted by the fluid on composite particles is likely the most important fluid-particle interaction that needs to be specified because of the importance of the drag force in initiating and sustaining bedload transport. For the composite particles the projected area of the particle to the flow will change as the particle tumbles

along the bed. Calculating the instantaneous projected area of the composite particle to the flow at every time step is possible with the information readily available during simulations. It is likely that some representative constant value between the maximum and minimum projected area will be an adequate approximation. Simulations need to be performed to determine the effect of different choices of the cross sectional area on net transport rates before the most efficient method of calculating the drag force is determined.

5.6.2. Settling Velocity

The problem of determining the settling velocity of composite particles is a difficult one that is closely related to the problem of specifying the drag force. When natural particles are allowed to settle through a fluid, such as water, they may twist, tumble and oscillate. The reason is that particles settling through a fluid attempt to orient themselves with their maximum projected area normal to the direction of the flow [*see Middleton and Southard*, 1984]. The result may be that during settling, the magnitude of the instantaneous velocity of a particle is greater than the average settling velocity. Considering that the focus of the model application is to high concentration bedload transport it is likely that the torques generated through collisions with other particles will dominate in magnitude over any torques that may be generated solely through fluid-particle interaction.

5.7. Conclusions

The new model presented here will increase the range of applicability and refine predictions of the discrete particle modeling approach to the bedload transport problem. Immediately, the composite particle modification may be used to study a wide range of

industrial flows, particularly where the specific gravity of the particles is large and the effects of the interstitial fluid can be ignored.

BIBLIOGRAPHY

Albert, R., I. Albert, D. Hornbaker, P. Schiffer, and A.L. Barabasi, Maximum angle of stability in wet and dry spherical granular media, *Physical Review E*, *56* (6), R6271-R6274, 1997.

Allen, M.L., The effect of particle proximity on the drag force generated at high reynolds numbers, *Transactions of the Institution of Chemical Engineers*, *58*, 187-194, 1980.

Bagnold, R.A., Experiments on a gravity-free dispersion of large solid spheres in a newtonian fluid under shear, *Proceedings of the Royal Society of London*, *A225*, 49-63, 1954.

Bagnold, R.A., The Flow of Cohesionless Grains in Fluids, *Philosophical Transactions of the Royal Society of London Series a-Mathematical and Physical Sciences*, *249* (964), 235-&, 1956.

Bagnold, R.A., Mechanics of marine sedimentation, in *The Sea*, edited by M.N. Hill, pp. 507-528, Wiley-Interscience, New York, 1963.

Bagnold, R.A., An approach to the sediment transport problem from general physics, *U. S. Geological Survey Professional Paper*, *422* (I), 1-37, 1966.

Bailard, J.A., An energetics total load sediment transport model for a plane sloping beach, *Journal of Geophysical Research-Oceans and Atmospheres*, *86* (C11), 938-954, 1981.

Bailard, J.A., and D.L. Inman, An energetics bedload model for a plane sloping beach - local transport, *Journal of Geophysical Research-Oceans and Atmospheres*, *86* (C3), 2035-2043, 1981.

Barabasi, A.L., R. Albert, and P. Schiffer, The physics of sand castles: maximum angle of stability in wet and dry granular media, *Physica A*, *266* (1-4), 366-371, 1999.

Batchelor, G.K., *An introduction to fluid dynamics*, 615 pp., Cambridge University Press, Cambridge, 1967.

Blatt, H., G. Middleton, and R. Murray, *Origin of Sedimentary Rocks*, Prentice-Hall, Inc., Englewood Cliffs, New Jersey, 1972.

Bowen, A.J., Simple models of nearshore sedimentation; beach profiles and longshore bars, in *The Coastline of Canada, Geological Survey of Canada Paper 80-10*, edited by S.B. McCann, pp. 1-11, 1980.

Calantoni, J., and T.G. Drake, Discrete-particle model for nearshore bedload transport, *EOS Trans. AGU*, *79* (17), S122, 1998a.

Calantoni, J., and T.G. Drake, Effect of fluid acceleration on bedload sediment transport in the surf zone, *EOS Trans. AGU*, *79* (45), F416, 1998b.

Calantoni, J., and T.G. Drake, Discrete-particle model for bedload transport: application to the equilibrium beach profile problem, in *Proceedings of the International Association of Hydraulic Research Symposium on River, Coastal and Estuarine Morphodynamics*, pp. 5-12, Genoa, Italy, 1999.

Church, J.C., and E.B. Thornton, Effects of breaking wave-induced turbulence within a longshore-current model, *Coastal Engineering, 20* (1-2), 1-28, 1993.

Conley, D.C., and D.L. Inman, Field observations of the fluid-granular boundary layer under near-breaking waves, *Journal of Geophysical Research, 97* (C6), 9631-9643, 1992.

Cundall, P.A., and O.D.L. Strack, A discrete numerical model for granular assemblies, *Geotechnique, 29*, 47-65, 1979.

Damgaard, J.S., R.J.S. Whitehouse, and R.L. Soulsby, Bed-load sediment transport on steep longitudinal slopes, *Journal of Hydraulic Engineering-ASCE, 123* (12), 1130-1138, 1997.

Dean, R.G., Equilibrium beach profiles: U.S. Atlantic and Gulf Coasts, Dept. of Civil Engineering, University of Delaware, 1977.

Dietrich, W.E., Settling Velocity of Natural Particles, *Water Resources Research, 18* (6), 1615-1626, 1982.

Dingler, J.R., and D.L. Inman, Wave-formed ripples in nearshore sands, in *Proceedings, Fifteenth Coastal Engineering Conference, July 11 - 17, 1976, Honolulu, Hawaii, American Society of Civil Engineers, New York*, pp. 2109-2126, ASCE, Honolulu, Hawaii, 1976.

Drake, T.G., and J. Calantoni, Discrete particle model for sheet flow sediment transport in the nearshore, *Journal of Geophysical Research-Oceans, 106* (C9), 19859-19868, 2001.

Drake, T.G., R.L. Shreve, W.E. Dietrich, P.J. Whiting, and L.B. Leopold, Bedload transport of fine gravel observed by motion-picture photography, *Journal of Fluid Mechanics, 192*, 193-217, 1988.

Drake, T.G., R.L. Shreve, and J.M. Nelson, Particle and fluid velocities in a bedload layer, *EOS Transactions AGU, 72*, 229, 1991.

Drake, T.G., and O.R. Walton, Comparison of experimental and simulated grain flows, *Journal of Applied Mechanics, 62* (1), 131-135, 1995.

Einstein, H.A., The bed-load function for sediment transportation in open channel flows, U.S. Department of Agriculture, Tech. Bulletin No. 1026, 1950.

Elgar, S., Relationships Involving 3rd Moments and Bispectra of a Harmonic Process, *IEEE Transactions On Acoustics Speech and Signal Processing, 35* (12), 1725-1726, 1987.

Elgar, S., and V. Chandran, Higher-order spectral-analysis of chua circuit, *IEEE Transactions On Circuits and Systems I-Fundamental Theory and Applications*, *40* (10), 689-692, 1993.

Elgar, S., E. Gallagher, and R.T. Guza, Nearshore sandbar migration, *Journal of Geophysical Research-Oceans*, *106* (C6), 11623-11627, 2001.

Elgar, S., and R.T. Guza, Nonlinear model predictions of bispectra of shoaling surface gravity-waves, *Journal of Fluid Mechanics*, *167*, 1-18, 1986.

Elgar, S., R.T. Guza, and M.H. Freilich, Eulerian measurements of horizontal accelerations in shoaling gravity-waves, *Journal of Geophysical Research-Oceans*, *93* (C8), 9261-9269, 1988.

Faria, A.F.G., E.B. Thornton, T.P. Stanton, C.V. Soares, and T.C. Lippmann, Vertical profiles of longshore currents and related bed shear stress and bottom roughness, *Journal of Geophysical Research-Oceans*, *103* (C2), 3217-3232, 1998.

Feddersen, F., R.T. Guza, S. Elgar, and T.H.C. Herbers, Alongshore momentum balances in the nearshore, *103* (C8), 15667-15676, 1998.

Foerster, S.F., M.Y. Louge, A.H. Chang, and K. Allia, Measurements of the collision properties of small spheres, *Physics of Fluids*, *6* (3), 1108-1115, 1994.

Fredsoe, J., and R. Deigaard, *Mechanics of Coastal Sediment Transport*, 369 pp., World Scientific, 1992.

Gallagher, E.L., S. Elgar, and R.T. Guza, Observations of sand bar evolution on a natural beach, *Journal of Geophysical Research-Oceans*, *103* (C2), 3203-3215, 1998.

Gilbert, G.K., The transportation of debris by running water, *U.S. Geological Survey Professional Paper 86*, 263 pp., 1914.

Goldstein, H., *Classical Mechanics*, Addison-Wesley Publishing Company, 1980.

Guza, R.T., and E.B. Thornton, Local and shoaled comparisons of sea surface elevations, pressures and velocities, *Journal of Geophysical Research*, *85C*, 1524-1530, 1980.

Haff, P.K., Grain Flow As a Fluid-Mechanical Phenomenon, *Journal of Fluid Mechanics*, *134* (SEP), 401-430, 1983.

Haff, P.K., and R.S. Anderson, Grain scale simulations of loose sedimentary beds - the example of grain-bed impacts in aeolian saltation, *Sedimentology*, *40* (2), 175-198, 1993.

Hanes, D.M., Grain flows and bed-load sediment transport - review and extension, *Acta Mechanica*, *63* (1-4), 131-142, 1986.

Hanes, D.M., and A.J. Bowen, A granular-fluid model for steady intense bed-load transport, *Journal of Geophysical Research-Oceans*, *90* (C5), 9149-9158, 1985.

Hopkins, M.A., W.D. Hibler, and G.M. Flato, On the numerical-simulation of the sea ice ridging process, *Journal of Geophysical Research-Oceans*, *96* (C3), 4809-4820, 1991.

Hsu, T.-J., A Two-Phase Flow Approach for Sediment Transport, dissertation thesis, Cornell University, 2002.

Inman, D.L., and R.A. Bagnold, Littoral processes, in *The Sea*, edited by M.N. Hill, pp. 529-553, Wiley-Interscience, New York, 1963.

Inman, D.L., M.H.S. Elwany, and S.A. Jenkins, Shorerise and Bar-Berm Profiles On Ocean Beaches, *Journal of Geophysical Research-Oceans*, *98* (C10), 18181-18199, 1993.

Irish, J.D., A.E. Hay, P. Traykovski, A. Newhall, R. Craig, and W.M. Paul, On attaching acoustic imaging instrumentation to the LEO-15 observatory for sediment transport and bottom boundary layer studies, *IEEE Journal of Oceanic Engineering*, *27* (2), 254-266, 2002.

Jaeger, H.M., C.H. Liu, and S.R. Nagel, Relaxation at the Angle of Repose, , *62* (1), 40-43, 1989.

Jenkins, J.T., and D.M. Hanes, A collisional regime in bedload transport, *EOS, Trans. AGU*, *73* (43), 282, 1992.

Jenkins, J.T., and D.M. Hanes, A sheared layer of colliding grains driven from above by a turbulent fluid, *EOS, Trans. AGU*, *74* (43), 320, 1993.

Jenkins, J.T., and D.M. Hanes, Collisional sheet flows of sediment driven by a turbulent fluid, *Journal of Fluid Mechanics*, *370*, 29-52, 1998.

Jenkins, J.T., and S.B. Savage, A Theory For the Rapid Flow of Identical, Smooth, Nearly Elastic, Spherical-Particles, *Journal of Fluid Mechanics*, *130* (MAY), 187-202, 1983.

Jiang, Z., and P.K. Haff, Multiparticle simulation methods applied to the micromechanics of bed-load transport, *Water Resources Research*, *29* (2), 399-412, 1993.

King, D.B., Studies in oscillatory flow bedload sediment transport, 184p., Ph.D. Dissertation thesis, University of California San Diego, 1991.

Kovacs, A., and G. Parker, A New Vectorial Bedload Formulation and Its Application to the Time Evolution of Straight River Channels, , *267*, 153-183, 1994.

Landau, L.D., and E.M. Lifshitz, *Course of theoretical physics*, 539 pp., Pergamon Press, 1987.

Luding, S., E. Clement, A. Blumen, J. Rajchenbach, and J. Duran, Anomalous energy-dissipation in molecular-dynamics simulations of grains - the detachment effect, *Physical Review E*, *50* (5), 4113-4122, 1994.

Madsen, O.S., Stability of a Sand Bed Under Breaking Waves, in *Proceedings of the 14th International Conference on Coastal Engineering*, pp. 776-794, 1974.

Madsen, O.S., Mechanics of cohesionless sediment transport in coastal waters, *Coastal Sediments*, 15-27, 1991.

Marion, J.B., and S.T. Thornton, *Classical Dynamics of Particles & Systems*, Harcourt Brace, Jovanovich, Publishers, 1988.

Meyer-Peter, E. and Müller, R., Formulas for bed-load transport, in *Rep. 2nd Meet. Int. Assoc. Hydraul. Struct. Res.*, Stockholm, pp. 39-64, 1948.

Middleton, G.V., and J.B. Southard, *Mechanics of sediment movement*, 401 pp., SEPM, Tulsa, Oklahoma, 1984.

Mindlin, R.D., and H. Deresiewicz, Elastic spheres under varying oblique forces, *ASME Journal of Applied Mechanics*, *21*, 237-244, 1953.

Nadaoka, K., and H. Yagi, Single-phase fluid modelling of sheet-flow toward the development of "numerical mobile bed", *Coastal Engineering*, 2346-2359, 1990.

Niño, Y., and M. Garcia, Gravel saltation .2. Modeling, *Water Resources Research*, *30* (6), 1915-1924, 1994.

Niño, Y., and M.H. Garcia, Experiments on particle-turbulence interactions in the near- wall region of an open channel flow: Implications for sediment transport, *Journal of Fluid Mechanics*, *326*, 285-319, 1996.

Ribberink, J.S., Bed-load transport for steady flows and unsteady oscillatory flows, *Coastal Engineering*, *34* (1-2), 59-82, 1998.

Ribberink, J.S., and A.A. Al-Salem, Sediment transport in oscillatory boundary-layers in cases of rippled beds and sheet flow, *Journal of Geophysical Research-Oceans*, *99* (C6), 12707-12727, 1994.

Richardson, J.F., and R.A. Meikle, Sedimentation and fluidization - Part IV: Drag force on individual particles in an assemblage, *Trans. I. Chem Engrs.*, *39*, 357-362, 1961.

Rowe, P.N., and G.A. Henwood, Drag forces in a hydraulic model of a fluidized bed -- part i., *Trans. I. Chem. Engrs.*, *39*, 43-54, 1961.

Ruessink, B.G., J.R. Miles, F. Feddersen, R.T. Guza, and S. Elgar, Modeling the alongshore current on barred beaches, *106* (C10), 22451-22463, 2001.

Schmeeckle, M.W., The mechanics of bedload sediment transport, Ph.D. Dissertation thesis, University of Colorado, 1998.

Sekine, M., and H. Kikkawa, Bedload transport on transverse slope. II, *Journal of Hydraulic Engineering-ASCE, 118*, 536-558, 1992.

Sekine, M., and G. Parker, Bed-Load Transport On Transverse Slope. I, *Journal of Hydraulic Engineering-ASCE, 118* (4), 513-535, 1992.

Sumer, B.M., A. Kozakiewicz, J. Fredsoe, and R. Deigaard, Velocity and concentration profiles in sheet-flow layer of movable bed, *Journal of Hydraulic Engineering-ASCE, 122* (10), 549-558, 1996.

Tennekes, H., and J.L. Lumley, *A first course in turbulence*, 300 pp., M.I.T. Press, Cambridge, Mass., 1972.

Thornton, E.B., R.T. Humiston, and W. Birkemeier, Bar/trough generation on a natural beach, *Journal of Geophysical Research-Oceans, 101* (C5), 12097-12110, 1996.

Traykovski, P., A.E. Hay, J.D. Irish, and J.F. Lynch, Geometry, migration, and evolution of wave orbital ripples at LEO-15, *Journal of Geophysical Research-Oceans, 104* (C1), 1505-1524, 1999.

Trowbridge, J., and O.S. Madsen, Turbulent wave boundary-layers .1. Model formulation and 1st-order solution, *Journal of Geophysical Research-Oceans, 89* (C5), 7989-7997, 1984a.

Trowbridge, J., and O.S. Madsen, Turbulent wave boundary-layers .2. 2nd-order theory and mass-transport, *Journal of Geophysical Research-Oceans, 89* (C5), 7999-8007, 1984b.

Wadell, H., Volume, Shape, and Roundness of Rock-Particles, *Journal of Geology, 40*, 443-451, 1932.

Walton, O.R., and Braun, R. L., Stress calculations for assemblies of inelastic spheres in uniform shear, *Acta Mechanica, 63*, 45-60, 1986a.

Walton, O.R., and Braun, R. L., Viscosity, granular-temperature, and stress calculations for shearing assemblies of inelastic, frictional disks, *Journal of Rheology, 30*, 949-980, 1986b.

Werner, B.T., and P.K. Haff, The impact process in eolian saltation: two dimensional simulations, *Sedimentology, 35*, 267 - 78, 1988.

Wiberg, P.L., and J.D. Smith, A theoretical model for saltating grains in water, *Journal of Geophysical Research, 90* (C4), 7341-7354, 1985.

Wilson, K.C., Analysis of bed-load motion at high shear stresses, *J. Hydr. Engrg., ASCE, 113*, 97-103, 1987.